CHALMERS
UNIVERSITY OF TECHNOLOGY

Noise Reduction of Mine and Tunnel Ventilation

Investigations on scale models and methods to determine noise reduction

Master's thesis in Sound and Vibration

SALLY BEENA ISABEL ARAND

DEPARTMENT OF ARCHITECTURE AND CIVIL ENGINEERING

CHALMERS UNIVERSITY OF TECHNOLOGY
Gothenburg, Sweden 2023
www.chalmers.se

Master's thesis 2023

Noise Reduction of Mine and Tunnel Ventilation

Investigations on scale models and methods to determine noise reduction

SALLY BEENA ISABEL ARAND

Department of Architecture and Civil Engineering
Division of Sound and Vibration
Chalmers University of Technology
Gothenburg, Sweden 2023

Noise Reduction of Mine and Tunnel Ventilation
Investigations on scale models and methods to determine noise reduction
SALLY B. ARAND

Supervisor: Oskar Lundberg, Epiroc Rock Drills AB
Supervisor: Renny Rantakokko, Epiroc Rock Drills AB
Examiner: Wolfgang Kropp, Chalmers University of Technology

Master's Thesis 2023
Department of Architecture and Civil Engineering
Division of Sound and Vibration
Chalmers University of Technology
SE-412 96 Gothenburg
Telephone +46 31 772 1000

Cover: The ventilation system of Epiroc AB.

Typeset in LaTeX
Printed by Chalmers Reproservice
Gothenburg, Sweden 2023

Noise Reduction of Mine and Tunnel Ventilation
Investigations on scale models and methods to determine noise reduction
SALLY B. ARAND
Department of Architecture and Civil Engineering
Chalmers University of Technology

Abstract

Ventilation systems used in mines and tunnels contain big axial flow fans, which dominate the sound environment together with the noise generated from heavy machinery. To fulfil the demands regarding work-placement and environmental regulations and with increasing awareness of noise induced health issues, the reduction of the emitted sound is investigated in a thesis project with practical measurements and simulations.
To do fast investigations a scale model of the ventilation system was designed. The fan scaling laws, which are used to scale fan properties between different fan sizes, showed, that by reducing the fan size and the rotational speed the fan performance will decrease highly. The resulting effect on the flow properties is rather small. The blade passage frequency will change, which leads to a change in the acoustic similarity. CFD simulations were performed in Comsol Multiphysics 6.1 to investigate the pressure and velocity field closely over a perforated plate and around a centrum-baffle, which are both part of the silencer of the ventilation system. The results showed a laminar-sublayer close to the wall and an increase in the fluctuations of the velocity and the pressure in the flow duct when adding the centrum-baffle.
In the practical part of the thesis the silencer of the ventilation system was scaled and its acoustic properties were determined with measurements. The transmission loss measurement methods were compared by using the two room method with microphones and a sound intensity probe. Both methods showed similar results. Insertion loss and level difference were measured in another setup. Overall there was no big difference between the silencer characteristics measured from the different methods. It was found that the most effective reduction is brought from the absorption material. The perforated plate does not add to the noise reduction.
At last an acoustic simulation for the silencer was set up in Comsol to investigate the transmission loss of the silencer further. Due to limitations in computational resources, the model is restricted to plane wave excitation, which limits the accuracy of the model and the possibility to directly compare the measurements with the simulation results. But both show the most effect due to the absorber and no added reduction by the perforated plate.

Keywords: mining, ventilation, transmission loss, silencer, pressure measurement, intensity measurement, CFD, FEM, scaling

List of Acronyms

Below is the list of acronyms that have been used throughout this thesis listed in alphabetical order:

AM	Acoustic Metamaterials
BPF	Blade Passage Frequency
CFD	Computational Fluid Dynamics
FEM	Finite Element Method
HVAC	Heating, Ventilation and Air Conditioning
IL	Insertion Loss
ISO	International Organization of Standardization
MPP	Micro-Perforated Panel
RR	Receiving Room
SR	Source Room
TL	Transmission Loss

Nomenclature

Below is the nomenclature of indices, sets, parameters, and variables that have been used throughout this thesis.

Indices

1	known fan
2	unknown fan
avg	average
D	dipole
in	incident
M	monopole
RR	receiving room
SR	source room
tr	transmitted
w	with silencing treatment
wo	without silencing treatment

Symbols

A	equivalent absorption area in m^2
D	fan size in m, (in Figure 4.7: diameter in m)
F	force in N
He	Helmholtz number
IL	insertion loss in dB
L	sound pressure level in dB relative to 2×10^{-5} Pa
L_I	sound intensity level in dB relative to $10^{-12}\,\mathrm{W/m^2}$
L_h	normalized sound attenuation in dB

Ma	Mach number
N	fan speed in revolutions per second
P	power in W
Q	volume flow in m^3/s
R	normalized flow resistivity
R_1	flow resistivity in $N \cdot s/m^4$ or $Pa \cdot s/m^2$
Re	Reynolds number
S	area of the cross-section of the duct in m^2
St	Strouhal number
T	reverberation time in s
TL	transmission loss in dB
U	piston velocity in m/s
V	room volume in m^3
W	sound power in W
Z_a	characteristic impedance of the porous material in N/m^2
a	center-to-center distance in m
c	speed of sound in m/s
c_L	speed of longitudinal structure waves in m/s
d	diameter in m, (in section 4.3.4: thickness in m)
d_h	hole diameter in m
f	frequency in Hz
f_c	critical frequency in Hz
f_R	ring-frequency in Hz
f_{St}	Strouhal frequency in Hz
h	radius of the passage in m
l	characteristic length in m
n	numeration: number of mesh points, microphone position etc.
p	pressure in Pa
t	time in s
u	velocity in m/s
x	location/ distance in m
Γ_a	propagation constant for the porous material

Γ_c	propagation constant for the coupled wave
η	normalized frequency
λ	wavelength in m
μ	absolute viscosity in $\mathrm{N \cdot s/m^2}$
ρ	density in $\mathrm{kg/m^3}$
σ	area porosity

Contents

List of Acronyms **vi**

Nomenclature **viii**

List of Figures **xv**

List of Tables **xix**

1 Introduction **1**
1.1 Background 1
1.2 Aim 2
1.3 Limitations 2
1.4 Specification of the issue being investigated 3

2 The Epiroc Ventilation System **5**
2.1 Measurement Results from previous Work 7

3 Literature Review **15**

4 Theory **19**
4.1 Noise Generation Mechanism 19
4.1.1 Flow Noise 19
4.1.2 Fan Noise 23
4.1.2.1 Fan Scaling Laws 24
4.1.2.2 Noise Generation around Fans 24
4.1.2.3 Sound from Fans in Ducts 26
4.2 Sound Propagation in Ducts 27
4.2.1 Breakin and Breakout Noise 28
4.3 Noise Mitigation Measures 29
4.3.1 Reactive and Resistive Silencer 29
4.3.2 Transmission and Insertion Loss 30
4.3.3 Silencer under flow conditions 31
4.3.4 Round Silencer 31
4.4 Fluid-Dynamic Scaling: Similitude 34

5 Design of the Scale Model **37**
5.1 The scale model 37

5.2 The expected Flow Properties and Fan Performance 40
5.3 Flow Study 41
5.3.1 The Geometry of the Simulation Model 42
5.3.2 Setup of the Flow Study 42
5.3.3 Simulation Results 43

6 Measurements with the Scale Model 49
6.1 Transmission Loss Measurements 49
6.1.1 Measurement equipment and setup of the measurement room . 49
6.1.2 Measurement Procedure 52
6.2 Measurement Results 53
6.2.1 Investigation of the measurement environment 54
6.2.2 Investigation of the measurement method 59
6.2.3 Behaviour of the Scale Model 64
6.3 Measurement of Insertion Loss 66
6.3.1 Conclusion on the Measurements 69

7 Acoustic Simulation 71
7.1 Setup of the Simulation Model 71
7.2 Simulation Results 73

8 Conclusion 79
8.1 Summary of the Findings 79
8.2 Future Work 80

Bibliography 83

List of Figures

2.1 The ventilation system of Epiroc [18] . . . 5
2.2 The ventilation system of Epiroc installed in a mine tunnel . . . 6
2.3 CAD model of the ventilation system . . . 6
2.4 The measurement positions for the ISO 3744 measurement of emitted sound power level . . . 7
2.5 The average sound pressure level in dBA of the measurement case with the perforated plate and the smooth plate . . . 8
2.6 The emitted sound power level in dBA of the measurement case with the perforated plate and the smooth plate . . . 9
2.7 The sound pressure level at the inlet and outlet of the ventilation system . . . 10
2.8 The TL of the PVC duct, which is placed downstream of the fan . . . 10
2.9 The total sound pressure level around the ventilation system . . . 11
2.10 The sound pressure level at 400 Hz (BPF) around the ventilation system 12
2.11 The IL of the standard silencer with circular perforations or with squared perforations . . . 12

4.1 Laminar and turbulent flow in a flow duct [1] . . . 19
4.2 Turbulent flow above a wall generates a laminar sub-layer [19] . . . 20
4.3 Description of the three ways in which flow and sound interact [24] . 20
4.4 Vortex shedding [17] . . . 22
4.5 Overview of Fan Noise [31] . . . 25
4.6 Leading and trailing edge noise [17] . . . 26
4.7 Equation of the cut-on frequency for different mode shapes [21] . . . 27
4.8 The breakin sound transmission loss from a rectangular metal duct: solid line describes measurement result and the points show predicted values [22] . . . 29
4.9 Typical reduction curve of a single wall [21] . . . 31
4.10 The TL for a Helmholtz resonator on a duct changes with different flow velocities[21] . . . 31
4.11 Computed normalized attenuation L_h over normalized frequency η for round silencer with a thickness-passage-ratio of 0.5 for different normalised flow resistivity values [22] . . . 32
4.12 Computed noise attenuation for A. no center body, B. rigid center body and C. absorbing center body [22] . . . 33

4.13 Attenuation of the round silencer with flow: (a) sound propagation in flow direction, (b) sound propagation against flow direction [22] . . 34

5.1 The scale model of the silencer 38
5.2 The pressure and velocity field of the silencer duct with an inlet flow velocity of 50 m/s 46
5.3 The pressure and velocity field of the silencer duct with the centrum-baffle in the flow with an inlet flow velocity of 50 m/s 47

6.1 Connection of the measurement equipment 50
6.2 Sketch of the measurement rooms and the source and microphone positions 51
6.3 The measurement rooms and the source and microphone positions . . 51
6.4 The measurement rooms and the source and microphone positions . . 52
6.5 Points for sound intensity measurement to determine the transmission from the duct wall 55
6.6 Setup to the study of the measurement environment: the gaps between the duct and the test window were sealed and the outlet was closed. In the source room the door to the test window was closed. . 56
6.7 Results to the study of the measurement setup regarding leakages and the distribution of the sound from the outlet opening of the duct 56
6.8 Results to the study of the measurement setup regarding leakages and the distribution of the sound from the outlet opening of the duct with correction 57
6.9 Results to the study of the measurement setup regarding leakages and the distribution of the sound from the outlet opening of the duct with adjustment to the average reverberation time 58
6.10 Comparison between the intensity scanning method and the point method for the measurement of the open duct sealed in the partition window 60
6.11 Comparison of the results obtained for the open sealed in duct with the pressure measurement and the two intensity methods 61
6.12 Comparison of the results obtained from the pressure and intensity method for the duct with absorber and the duct with absorber and perforated plate 61
6.13 Comparison of the results obtained for the open sealed in duct with the pressure measurement and the two intensity methods, the microphone on position 3 was excluded from the pressure results 62
6.14 Comparison of the results obtained from the pressure and intensity method for the duct with absorber and the duct with absorber and perforated plate, the microphone on position 3 was excluded from the pressure results 63
6.15 The comparison of the TL results from the pressure method of the scaled silencer model from duct to the added absorber and the duct with the absorber and the perforated plate 65

6.16 The comparison of the TL results from the intensity method of the scaled silencer model from duct to the added absorber and the duct with the absorber and the perforated plate 65
6.17 Sketch of the measurement rooms and the source and microphone positions for the second measurement 67
6.18 TL from the intensity scan at the inlet and outlet side of the duct . . 68
6.19 IL obtained from pressure and intensity measurements of the duct with absorber and the duct with absorber and perforated plate compared to the empty duct 68

7.1 The model of the acoustic simulation 71
7.2 Determination of the flow resistivity by comparison of measurement data and simulation results 73
7.3 TL result from the acoustic simulation model for the empty duct, the duct lined with absorber and the duct lined with absorber and the perforated plate. 74
7.4 The TL result of the simulation compared to the TL result from the pressure measured in the first measurement setup 76
7.5 The TL result of the simulation compared to the TL result from the intensity measured in the first measurement setup 76
7.6 The TL result of the simulation compared to the TL result from the intensity measured in the second measurement setup 77

List of Tables

2.1 Atmospheric conditions during the measurement 7

5.1 The dimensions of the AVH90 ventilation system and the scale model 38
5.2 The performance parameter and flow properties of the AVH90 ventilation system and the scale model 40

6.1 Atmospheric condition in the RR during the measurements 54
6.2 Reverberation time T_{60} in the receiving chamber 54

1 Introduction

1.1 Background

The company Epiroc Rock Drills AB, which is based in Sweden, develops and produces drill rigs, rock excavation and construction equipment and tools for surface and underground applications for the mining, infrastructure and natural resource industries all over the world.

An important product to make work in tunnels and mines possible and secure is a ventilation system. These are used to move out the toxic air like exhaust gas from vehicles with combustion engine or gas from explosives used to advance deeper into the rock. Ventilation fans deliver fresh air through ducts into the underground tunnels, which then push out the bad air through the tunnel entrance. With an efficient ventilation systems the productivity can be kept high and energy costs are kept low.

Typically a ventilation system from Epiroc consists of an inlet silencer, the fan and engine, guide vanes and an outlet silencer. The ventilation system can be purchased with variations in diameter. Also, the different fan sizes have different power sources. For a system with a diameter of 900 mm the total emitted sound power level is 116 dBA. This was measured following the ISO 3744 standard. For the measurement the ventilation system was set up with two standard silencers. The standard setup for the silencer is the duct lined with absorptive material and a perforated plate. The sound reduction can be improved further by installing a centrum-baffle. The fan was operated with 50 Hz.

The emitted sound levels are high and being exposed to high noise levels through a long period of time can lead to noise related health problems. Furthermore, the ventilation systems are usually placed at the entrance of a mine, so it is possible that surrounding areas are exposed to the ventilation noise.

The operators of a mine have a high responsibility to fulfill work-placement and environmental regulations on their construction site. Furthermore, the ability to provide a ventilation system with a low sound radiation gives a competitive advantage.

In this thesis work, it will be investigated, how a further noise reduction can be achieved and tested as the product is -due to its production in India- not easily available in Sweden.

1.2 Aim

Due to high emitted sound levels, workplace and environmental regulations and market competition, the possibility to further reduce the noise of the ventilation system was investigated in a master´s thesis project.

One important step was to find out about new noise mitigation measures in similar applications. Here topics addressing flow noise from ducts or fan noise were of interest.

Furthermore, a good way to investigate possible countermeasures experimentally had to be found because the ventilation system is difficult to procure and building new countermeasure concepts for just a first estimation on the performance can be costly.

Using a scaled model of the ventilation system was a possibility, which was further investigated.
The ventilation systems range from a diameter of 63 cm to 224 cm. The advantage of a scale model is that it is much smaller and handier than the full-size product and is easily available. The practical investigation of countermeasures can be done much faster and less costly. From the measurement result on the scale model it can be evaluated whether the reduction effect is sufficient to try the investigated sound reduction measure on the full-sized machine as well.

In order to have the scale model as a good representation of the ventilation system it needs to contain all its components: the silencers, the fan and motor and the guide vanes.

1.3 Limitations

However, it could not be achieved to recreate the complete ventilation system within the thesis project. The thesis project will focus one the representation of the silencer and the acoustic study of it without flow conditions.

The silencer was investigated experimentally with the built scale model and in a simulation. Both investigations were restricted to the study of its acoustic properties. The numerical investigation was further reduced to plane wave excitation of the duct due to limited computational resources. As the scale model so far consists of the silencer alone because the fan source had not been built in, no flow was introduced to the investigations. The fluid dynamic properties were only handled very roughly and theoretically in order to keep track of the changes, that would appear due to the scaling of the fan.

1.4 Specification of the issue being investigated

The very first question, that needed to be investigated, was about how the noise is generated in the ventilation system to identify the main noise sources.

Secondly, the common noise reduction measures were studied to see, which measures are already applied to the ventilation system and where room for new ideas and improvements is. For this new research papers with new design ideas were of interest.

Furthermore, the use of scaling models had to be investigated.
The use of a scaling model in order to have a quick and cost-saving option to do a fast measurement on noise mitigation measures only makes sense, if the scaled model is a valid representation of the actual product. The behaviour of the scale model should either be very similar to the actual ventilation system or in a way, that one knows exactly how it behaves different from the real case, so that a user can draw concrete and valid conclusions from the behaviour of the scaled model and how it might be different from the actual product.

One task during the thesis work was to find out, the best way to scale the ventilation system down and to still maintain a good representation of it. Here the most important characteristics were the flow and acoustic properties.

Hence, the effect of scaling on the fan and the related flow properties had to be investigated. One needed to know how the flow properties change when the dimensions like duct diameter or blade length are reduced and how they could be influenced to keep them constant if necessary.

Furthermore, the acoustic properties had to be investigated. In the product the silencer consists of a perforated plate and a cavity filled with absorptive glass wool. A decision here was whether the cavity depth, material and the size of the perforations needed to be scaled or if they could just be kept constant in its dimensions.

Constant variables could for example be the flow speed, pressure or some of the liner dimensions, like the size of the perforations or the cavity depth. If a measure targeting the blade passage frequency (BPF) is of interest, it is needed to adjust the number of blades in dependency with the used fan speed, so that the BPF is the same as in the full-sized ventilation system. Conversely this means, that one cannot just use the ventilation systems fan, because the number of blades might need to be adjusted.

The scale model as a tool can be extended by building a simulation model. The experimental test results of the scale model can be compared to the simulation results. If they have a good agreement, the difference in the behaviour to the full-sized machine can be calculated by solving the simulation model. From that one could make predictions from the simulations in the future as well.

After the building, measuring and analysing the differences between the scale model and the ventilation system, in a last step new possible noise mitigation measures, which can be investigated in the future are described.

2

The Epiroc Ventilation System

Figure 2.1: The ventilation system of Epiroc [18]

A ventilation system is an important part for the work in mines and tunnels. It assures a fresh air supply inside the mine. Without a ventilation system exhaust gas from vehicles and smoke from explosions cannot escape back to the tunnel exit, which would make the work in a mine or tunnel impossible.

In figure 2.1 and 2.3 the ventilation system is displayed. From the left to the right, the ventilation system goes from the inlet side, where air is sucked in, to the outlet side. On the inlet side is the bellmouth and then the inlet silencer. The inlet silencer duct, like the outlet silencer, is layered with absorptive material and a perforated plate. Furthermore, a centrum-baffle can be installed to the silencer to achieve further noise reduction. This can be seen in the CAD model in figure 2.3. Behind the inlet silencer is the fan motor and the axial flow fan, which moves the air into the ventilation duct. To straighten the flow, guiding vanes are installed behind the fan. Then the flow passes the outlet silencer before exiting into a vinyl duct, which is attached behind the ventilation system.

The ventilation system can be installed at the entrance to the mine or inside. When installed at the entrance of the mine, the axial flow fan can suck in the fresh air from the outside and deliver it deep into the mine. By that the polluted air gets pushed

out through the entrance. If the ventilation system is hanging inside the mine like in figure 2.2, the polluted air can for example be moved to another tunnel, which has a ventilation system connected with the outside.
It can be elevated by standing, for example, on a container or it can be hanged at the ceiling of the mine. This can be seen in figure 2.2.

Figure 2.2: The ventilation system of Epiroc installed in a mine tunnel

The ventilation system of Epiroc can be purchased in different sizes. For simplicity it was decided, that this thesis work should focus on scaling one of the available ventilation systems. Hence, the AVH90 machine will be in the focus of the thesis as there was already measurement data from previous work available. As hinted in the name, the AVH90 ventilation system has an inner duct diameter of 0.9 m. The silencer is 1.2 m long and consists of a 1 mm thick perforated plate. The perforated plate has 5 mm holes with 3 mm spacing between. Behind the perforated plate is a 7 cm cavity, which is filled with absorptive glass fibre wool. This standard silencer can be improved further with a centrum-baffle in the middle of the silencer. It also consists of glass fiber wool and a perforated plate.

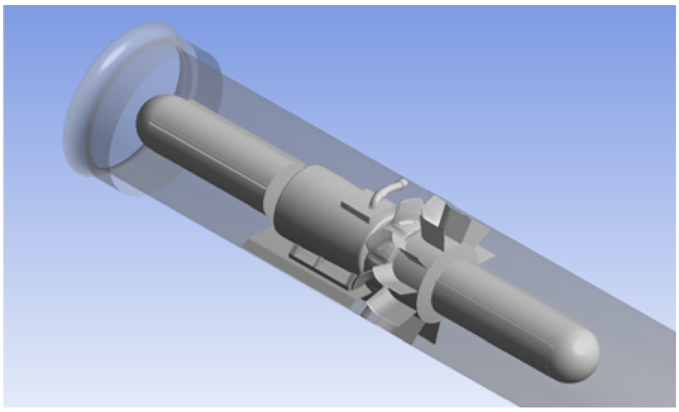

Figure 2.3: CAD model of the ventilation system

2.1 Measurement Results from previous Work

The measurements on the ventilation system to determine the emitted sound power were conducted following the standard ISO-3744, which describes the determination of emitted sound power of noise sources like machines in a free-field with one or more reflective planes [6]. The ventilation system was operated with 50 Hz, a total flow pressure of 1300 Pa and the blade angle was set to 44°.

The measurement positions are partly displayed in figure 2.4. There are 20 horizontal measurement positions around the ventilation system and 4 vertical positions, which differ in height. This pattern forms a grid of measurement positions around the machine. The total length of this measurement box is 7.8 m, it is 3.5 m wide and 2.8 m high.

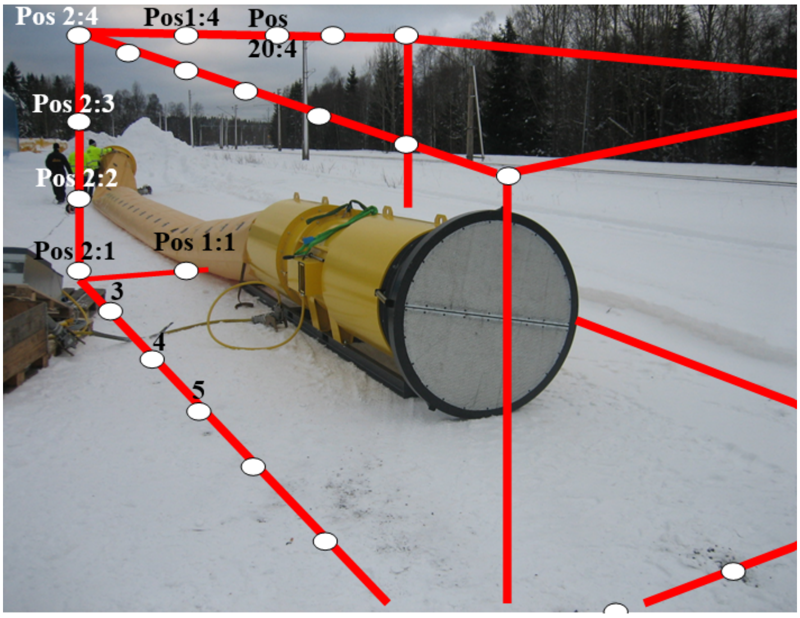

Figure 2.4: The measurement positions for the ISO 3744 measurement of emitted sound power level

The measurements were conducted with the SoftdB Concerto measurement system and 4 BSWA Microphones.

The environmental conditions are listed in table 2.1 below.

Table 2.1: Atmospheric conditions during the measurement

Temperature	$-5\,°C$
Humidity	85 %
Air pressure	1027 hPa
Wind	$4\,m\,s^{-1}$

In figure 2.4 the setup for the measurement case with the so-called super silencer of Epiroc is shown. The super silencer can be attached to the opening. The measurement results, which will be presented here, are from other measurement cases.

In the measurement cases presented here the ventilation system was set up in a standard way. So, its the silencer duct with the liner consisting of the perforated plate and 7 cm of absorptive material. The centrum-baffle, which can be positioned in the middle of the silencer, was not attached.
For the first measurement case the absorber and perforated plate was covered with a solid, flat plate. In the second case the hard plate was removed, so the setup could be measured in its standard way.
From the measurements the averaged and A-weighted sound pressure- and sound power level was analysed in the post-processing.

In figure 2.5 the averaged and A-weighted sound pressure level is displayed for the measurement case with the absorber and the perforated plate and the case, where the perforated plate is covered with a solid plate.
The results are obtained by averaging the sound pressure level over all 20 measurement positions.

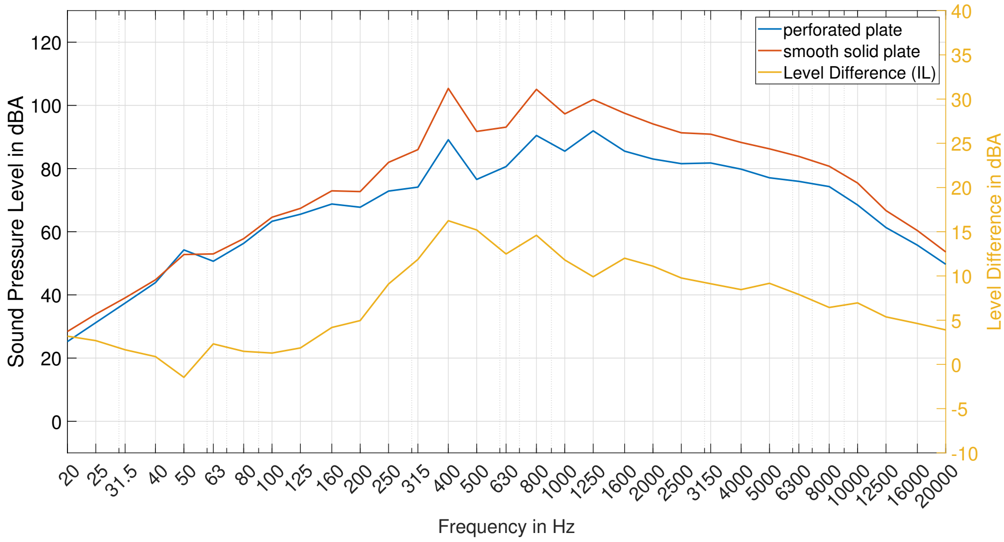

Figure 2.5: The average sound pressure level in dBA of the measurement case with the perforated plate and the smooth plate

Overall it can be observed, that the sound pressure level increases towards approximately 1250 Hz. Then the sound pressure level decreases towards higher frequencies. Four prominent maxima can be observed in the course of the curve. There is a maximum in the low frequency range at 50 Hz, which co-insides with the input power of the motor. The maxima at 400 Hz, 800 Hz and 1250 Hz go back to the BPF, which can be calculated by the operating frequency of the fan and the number of blades. The AVH90 has 8 fan blades and in this measurement case the fan was operated with 50 revolutions per second. So, one obtains 50 Hz $\cdot$ 8 blades = 400 Hz for the BPF. The other maxima go back to its harmonics. The noise from the fan goes back to the flow separation at the blades, which cause vortexes. The BPF is caused by the interaction of the blades and the guiding vanes. So, the most important contributors to the overall noise are the fan motor, the axial fan and turbulence in the flow.

If the fan speed would be reduced the noise level would decrease as well. The curve displayed in figure 2.5, would shift towards lower sound pressure level values and the maximum of the BPF would shift to lower frequencies.

Another observation that can be made is the impact of the absorber and the perforated plate. In the low frequency range until 125 Hz the difference between the curves is rather small. Above 125 Hz the difference increases with frequency up to a difference of about 15 dB. In the very high frequency range, the level difference is getting smaller again.
The difference between the curves was calculated by the level difference, which for this case is comparable to an insertion loss (IL) because its the difference between the untreated and treated ventilation duct.

From the sound pressure levels presented in figure 2.5 the total emitted sound power level was calculated by multiplying the sound pressure level values with an area factor of 19.6. The obtained results are shown in the figure 2.6.

From these values the total emitted sound power level can be calculated, which is 129.7 dBA for the measurement with the smooth hard plate and 116.7 dBA for the measurement with revealing the perforated plate and the absorber. So, the silencer with the absorption material and the perforated plate gives an overall noise reduction of 13 dB.

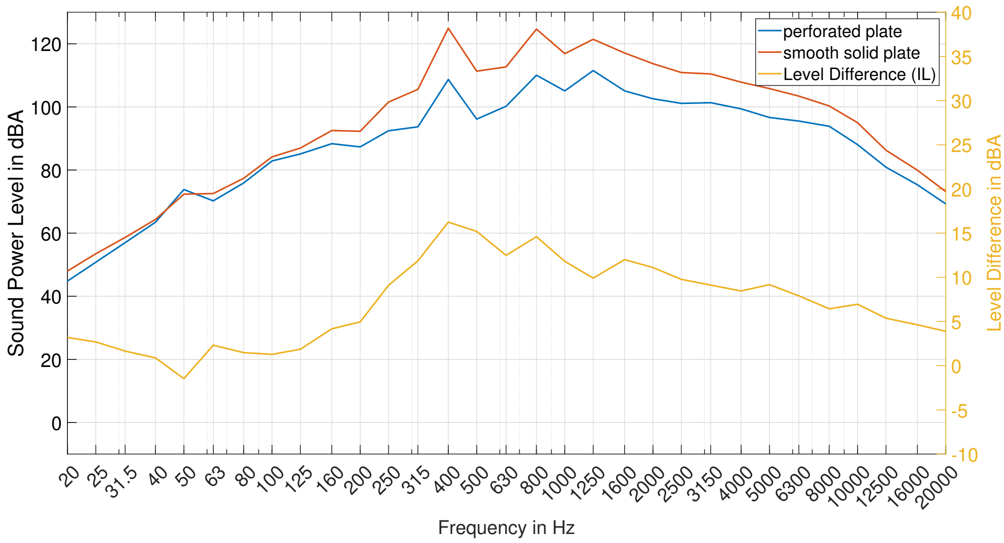

Figure 2.6: The emitted sound power level in dBA of the measurement case with the perforated plate and the smooth plate

In figure 2.7 the measured sound pressure level at position 10:2 (inlet) and 20:2 (outlet) are displayed (see positions in figure 2.4).

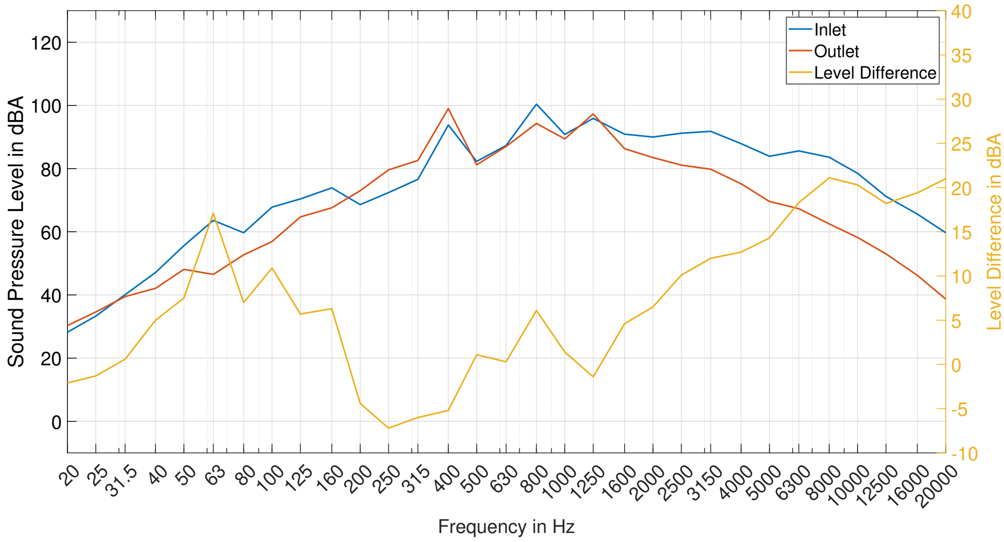

Figure 2.7: The sound pressure level at the inlet and outlet of the ventilation system

It can be observed that the inlet noise is higher in the frequency range below 160 Hz and above 1600 Hz. This can also be observed in the summation of the sound pressure level values. For the inlet side the total sound pressure level is 104.2 dBA. For the outlet side its 102.7 dBA. So, when taking the sum the difference is rather small. Just like in the previously presented results, the range from 400 Hz to 1250 Hz is dominated by the noise of the BPF.

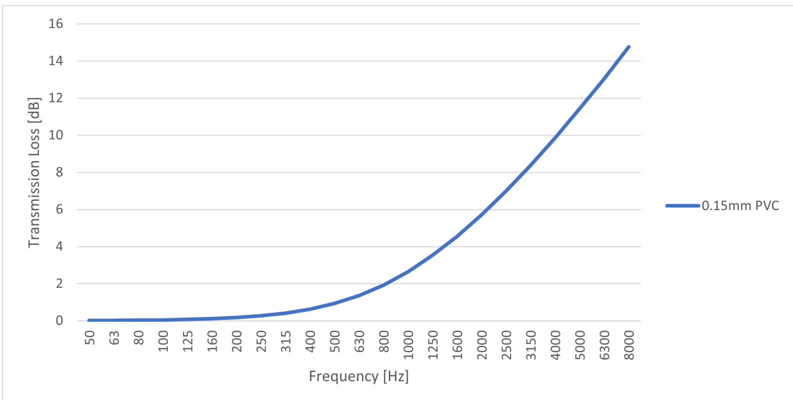

Figure 2.8: The TL of the PVC duct, which is placed downstream of the fan

The level difference in the frequency range above 1.6 kHz is created by the vinyl duct. It can be seen in figure 2.4. In figure 2.8 the transmission loss (TL) of the duct is displayed. It has no reduction properties until 400 Hz. Then the values increase with frequency. Its similar to the level difference shown in figure 2.7. Up to

1.6 kHz the level difference is different to the TL since the levels are dominated by the harmonics of the motor and the blade. But above the level difference increases with frequency and shows similar behaviour to the TL of the vinyl duct.

In figure 2.9 the total A-weighted sound pressure level is shown for all positions around the ventilation system. Each curve represents a different measurement height. The positions 1 to 20 are displayed in a way, that the outlet position of the ventilation system is at the top in figure 2.9. Position 10, the inlet, is at the lower end.

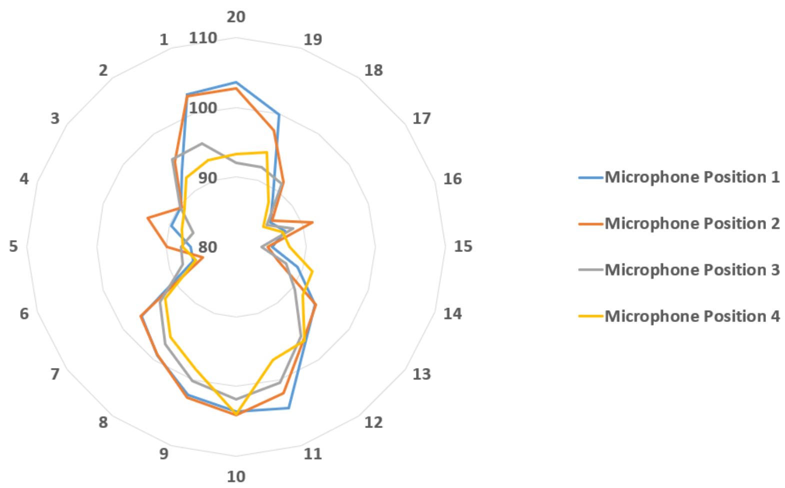

Figure 2.9: The total sound pressure level around the ventilation system

It can be observed, that at height 3 and 4, which were around 1.9 m and 2.8 m high, lower sound pressure levels were measured than at position 1 and 2, which were floor level and approximately at 0.9 m height. During the measurement position 3 and 4 were shielded on the inlet side, which leads to the level difference in the results.

Another aspect, that can be observed is that the sound pressure level is highest at the inlet and outlet position. Around the ventilation system the sound pressure level is in a range between 80 dBA to 90 dBA, while at the openings the level goes up over 100 dBA. Especially from position 5 to 6 and 5 to 4, respectively 15 to 16 and 15 to 14, it can be seen that the sound pressure level decreases significantly. The increase toward position 5 and 15 is most likely due to the fan and motor. From the radar chart it can be seen, that the ventilation system almost radiates like a dipole sound source.

To compare, the sound pressure level at the measured positions for the BPF at 400 Hz are displayed in figure 2.10. It can be observed, that especially at the outlet side, the sound pressure level of the frequency component is almost equally strong as the total sound level in figure 2.9.

The high noise level from the inlet and outlet opening stresses the need of noise reduction measures on those sides. Especially when the ventilation system is placed at the entrance of a mine, the radiation into the environment is high and might cause problems with noise regulations.

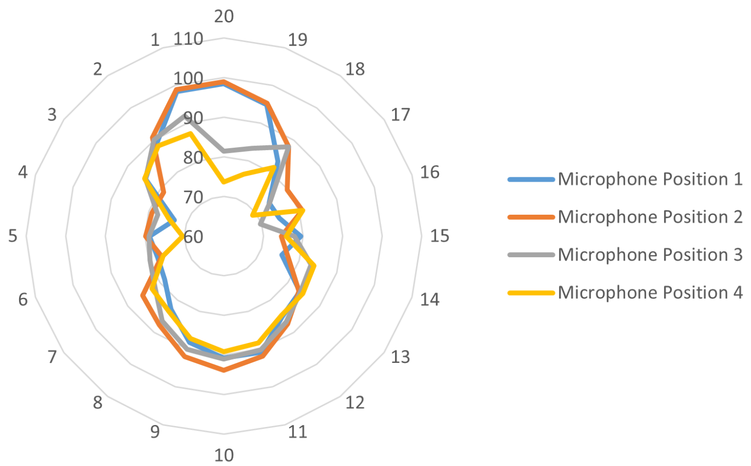

Figure 2.10: The sound pressure level at 400 Hz (BPF) around the ventilation system

At last an investigation on the perforation holes was performed. The circular perforation holes were compared to squared perforations. In figure 2.11 the result is displayed by the IL. The untreated comparison case to calculate the IL is the measurement case with the solid reflective plate covering the silencer. In figure 2.11 the 'original silencer' represents the measurement with the circular perforations, while 'new silencer' shows the results to the measurements with the squared holes.

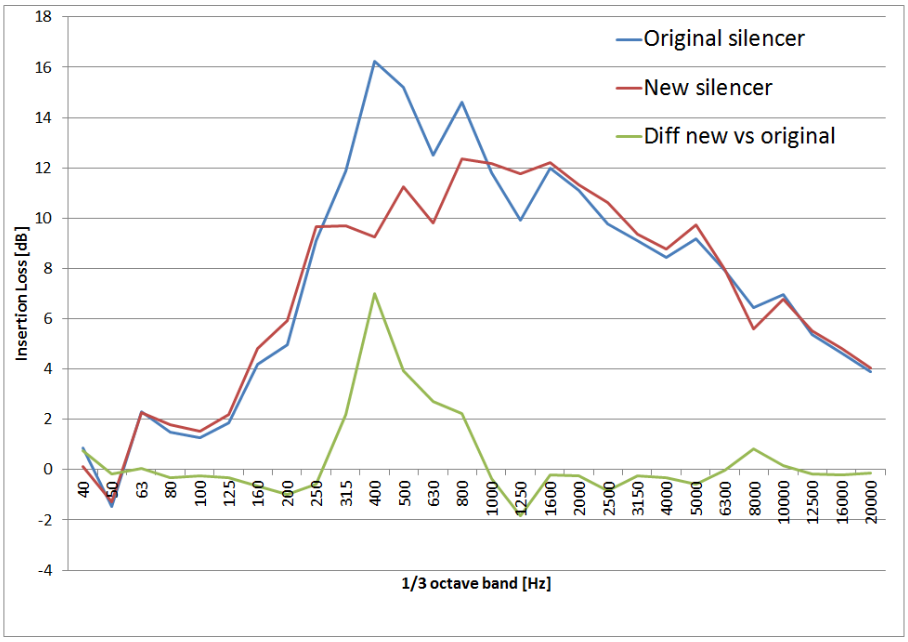

Figure 2.11: The IL of the standard silencer with circular perforations or with squared perforations

From the difference between the IL (green curve) it can be observed, that the circular perforations contributes most to the reduction in the frequency range of 250 Hz to 1 kHz with a strong maximum at 400 Hz, the BPF.

3
Literature Review

The literature review was focused on primary and secondary measures to reduce the emitted sound from ventilation ducts. In the following, papers investigating ideas on silencers or fan design are described. Fan and flow noise reduction is a big issue in many applications. There are investigations for air condition, heating and ventilation systems for vehicles, buildings, electric devices and aeroplanes. There are many studies that can be found, so presented here are only some of many solutions. Another topic of interest, was the scaling of the fan size and the prediction of the performance parameters using the fan scaling laws.

In the article [2] the sound generation and the noise treatment on ventilation ducts is summarized. The sound emitted from a ventilation system has many contributors. At first there is the sound emitted from the operating motor of the fan. Further sound generation is due to the propagation of turbulent flow in the duct. The turbulent flow in the duct excites the duct walls, which leads to breakout noise, which is radiated into the surrounding environment. And another contributor is the fan noise, which generates noise due to its interaction with the turbulent flow. The BPF, a harmonic noise component, is generated when the axial fan blades pass the flow guiding vanes. The noise reduction measures stated in the article are the installation of silencers on the inlet and outlet side of the flow fan. To reduce the breakout noise, the duct wall can be encapsulated by a layer of isolating material. And another solution they propose is layering the fan housing from the inside with absorptive material.

In other papers further noise reduction measures, that have been studied in the past, are summarized as well.

In [25] changes on the leading edge to reduce fan noise were for example the serration of the blade´s leading edge. Other reduction measures used "flow-permeable or porous materials" on the blade to achieve sound mitigation.
To reduce the leading edge noise the authors of the research project [25] studied fan blades with differently shaped perforations on the leading edge. Their results showed a sufficient effect on the noise level, but they lost some of the fan´s performance.

Passive acoustic treatments are mentioned in [34], like acoustic liners. Further primary measures for the reduction of fan noise include the irregular arrangement of the blades to reduce tonal noise. The author also mentions serrated blades, which reduce the vortex shedding noise. In addition to that the use of porous material or even the use of an add-on structure with a pattern following the structure of shark skin were proven to have satisfying noise reduction properties. Furthermore, the use of micro-perforated panels (MPP) is mentioned.

Another approach to get noise reduction is the use of reduction measures, which have a high absorption for a certain resonance frequency, like Helmholtz or quarter-wavelength resonators or MPP. [20]

A new petal-shaped silencer design was introduced in the paper [30]. The authors compared its acoustic and aerodynamic properties numerically against usual silencer solutions, like cylindrical and radial silencers. The advantage of their design was, that besides absorption also reflection added to the sound reduction. Both aerodynamic and acoustic results showed an advantage towards the circular and radial silencer.

For noise reduction at low frequencies the authors presenting their work in the paper [15], designed a silencer part, that can be attached to a ventilation duct, which consists of many different Helmholtz resonators. The Helmholtz resonators on the array are different in their dimensions, so that they have different resonance frequencies, which results in a broader TL. The investigations are made for the low frequency region of plane wave propagation and do not include the effect of an airflow in the duct. But according to the authors, the presented results will hold for low speed flows. The different prototypes reached TL values between 20 dB and 30 dB or 10 dB to 20 dB in a frequency range between 800 Hz to 1600 Hz.

In the following research [20] the authors explored "eight periodically arranged varying-depth units", which contain a porous acoustic meta-material (AM) regarding "broadband noise reduction in flow ducts". An array of this eight units can be integrated like a panel absorber to a duct wall. Numerical and experimental tests showed a TL of over 20 dB in a frequency range of 1.5 kHz to 3 kHz. The high sound absorption is generated by the transformation of the incident wave to a surface wave and the properties of the porous material.

A duct lined with a MPP and an air cavity behind is investigated in [16]. The authors see the advantage of this absorber (MPP plus air cavity) in the fact, that it has low influence on the flow and fan characteristics. Furthermore, one can gain a high noise reduction due to the change in the cross section and high particle velocity in the MPP. 16 dB of fan noise reduction could be achieved.
The size of the cavity can be fitted to a critical frequency range, so that the highest reduction is obtained for a certain frequency range, like for example the BPF.
Another finding, which induced additional high-frequency content in the measurement results, was the placement of the fan inside the lined duct section. The air flowing through the holes lead to high-frequency noise. This could be avoided by placing the absorber in front of the fan.

Another research [32] investigated the use of petal-shaped perforations instead of the common circular perforations of MPP. The authors studied the absorption of the petal-shaped perforation and the traditional hole using the finite element method (FEM). The change of the flow velocity and flow resistivity of the petal-shaped hole leads to a higher absorption.

In the research [34] the reduction of the BPF and its first harmonic is achieved by adding 3D printed acoustic treatment parts above the fan. The authors have designed these components by 3D printing AM in a maze-like setup, which is fitted to a certain resonance frequency. With the acoustic treatment the primary sound field is canceled out. The high advantage of this solution is, that the treatment can be designed for any frequency and does not need much space.

In the next study [33] the authors investigated the noise generated by vortex shedding at the tip of propeller blades. Using computational methods they studied 2 classical propeller with different blade numbers and a conceptual propeller, which consists of six bent blades, which are joined at the end, so that the propeller consists of 3 joined blades. They found out, that even though the vortex development is different, there is no advantage in the emitted noise level by using the conceptual blade. Furthermore, the results showed, that between the two classical blade designs, the one with 6 instead of 3 blades, was much quieter. The vorticity magnitudes were lower. From their study the authors concluded, that a "trade-off" can be made between the propeller design and the "aerodynamic performance".

A new MIT study [14] presented a so-called toroidal propeller design, which gives much advantages regarding the emitted noise. This design was tested as an alternative for common drone propellers. Instead of having separate single blades, the toroidal propeller blades are looped, which gives a broad noise reduction between 1 kHz to 5 kHz. The author explains, that this goes back to the distribution of the vortexes, which are created by the propeller blades. With the toroidal propeller they are spread over the whole blade geometry instead of being restricted to the tip only. With that they attenuate faster in the air and do not travel all the way to an observer.

The next study [12] is not about possible new designs to reduce duct or fan noise, but investigates the fan scaling laws. In the study a fan with a diameter of 10.36 m is scaled down to 1.25 m. The authors conducted detailed Computational Fluid Dynamics (CFD) simulations and experimental investigations on the full-sized and the scaled fans to determine whether the fan scaling laws adequately describe the power, pressure and fan efficiency. Their results showed quite a good agreement between the experimental and numerical results for the scaled fans and between the scaled and full-sized fan. The result for the experimental fan power of the scaled fan, which was determined experimentally, was only 6 % to 9 % higher than the numerically investigated power of the full-sized fan. As a consequence the fan efficiency in the simulation is also a little higher. The authors concluded, that the overall agreement is good and that the fan efficiency can be predicted within 5 % certainty.

4

Theory

In the following chapter the theory necessary for explaining the noise generation of the ventilation system is described. Furthermore, the sound propagation inside the duct system is explained. At last general noise mitigation measures are presented.

4.1 Noise Generation Mechanism

The two sound sources contributing most to the sound of the ventilation system are the air flow and the fan. In the following the noise generation is described.

4.1.1 Flow Noise

Sound generated by discontinuities in an air flow is called aerodynamic noise or more generally for any medium just flow noise. [17]

There are two different kinds of flow, which are distinguished. There is laminar and turbulent flow. Gas or liquid travelling with low velocity can usually be described as laminar flow. Laminar flow is characterised by the fluid particles traveling along straight parallel paths. When the propagation speed of the medium is increased, the propagation paths of the particles are no longer straight, but get mixed up and interfere each other. The velocity changes on every point. [13]
This is sketched in figure 4.1.

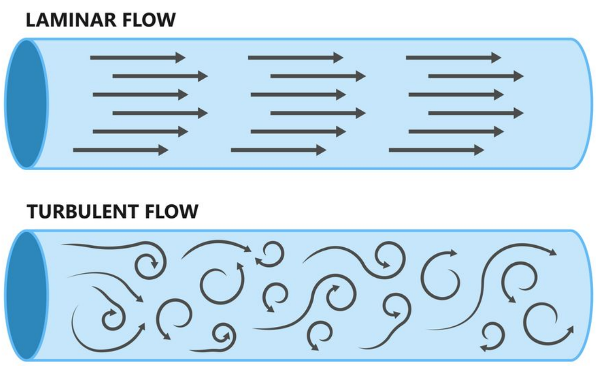

Figure 4.1: Laminar and turbulent flow in a flow duct [1]

The Reynolds number Re is used to distinguish between laminar and turbulent flow.

The Reynolds number is calculated from the "ratio of the magnitude" of the inertia forces and the viscous forces. In equation 4.1 the calculation of the Reynolds number for round flow ducts is shown. The calculation is made from the fluid density ρ, the flow velocity u and the diameter of the pipe d. In the denominator the absolute viscosity μ is inserted.

$$Re = \frac{\rho u d}{\mu} \tag{4.1}$$

As an example of how the result for the Reynolds number can give an indication of whether the flow is turbulent or laminar, the authors stated, that for a flow duct a Reynolds number of 2000 indicates a laminar flow, while a Reynolds number above 4000 is characteristic for turbulent flow conditions. [13]

For high Reynolds numbers the flow propagation in pipes depends on the surface roughness of the pipe. Usually flow in ducts is turbulent. Close to the boundary there always is a very thin layer, where the flow is laminar. This very thin region is called viscous or laminar sub-layer. With increasing Reynolds number the size of the sub-layer will decrease further. [13] Close to the wall the flow velocity decreases to zero. [19]

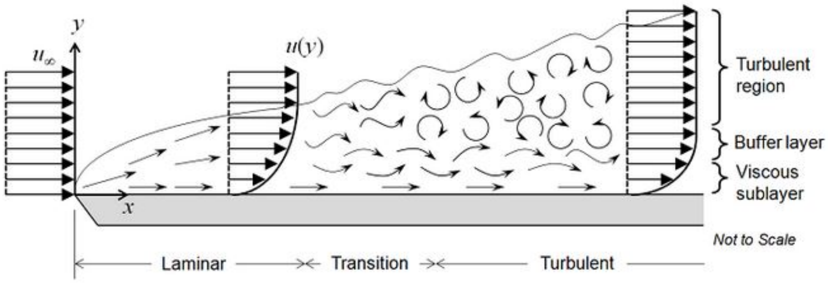

Figure 4.2: Turbulent flow above a wall generates a laminar sub-layer [19]

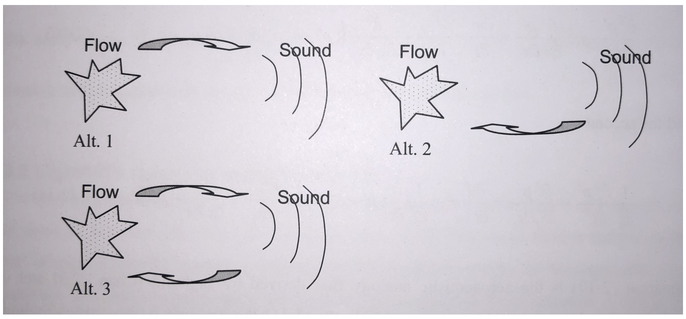

Figure 4.3: Description of the three ways in which flow and sound interact [24]

Turbulence or "unsteady fluid flow" causes noise generation. [17]
There are three ways in which an acoustic field interacts with a flow field. They are sketched in figure 4.3 .

Firstly, there is sound generation from turbulence, which was first described by Lighthill. [24] He found out, that the turbulent fluid acts on a surrounding acoustic medium at rest in the same way as a quadropole source.
The varying pressure field in the turbulent flow is divided by a near field pressure field, which stays with the turbulence and a far field, which propagates away from the turbulence taking a small portion of the energy along, which is the flow noise. [17]

Secondly, there also is the possibility of the acoustic field affecting the flow field. This can, for example, happen at sharp edges, where the flow is separated. The flow separation leads to vortex shedding, which is further described in the following text. [24]

And the third type of interaction leads to whistling noise. This appears, when an acoustic mode interacts with a natural oscillation. The sound and the flow generate a self-sustaining oscillation. [24]

There are three source terms, that can be derived by Lighthill´s theory.

For a monopole source application examples are loudspeakers in a box, which is small in comparison to the wavelength λ. Furthermore, the inlet or outlet opening of a pipe -like for example exhaust pipes- can be described by a monopole source. This applies only for low Mach number Ma flows though. [24]

The Mach number Ma is one of a few dimensionless parameters in the aeroacoustic field. The Mach number is calculated from the ratio of the flow speed u and the speed of sound c.

$$Ma = \frac{u}{c} \tag{4.2}$$

For flow noise induced by unsteady flow, a small Ma indicates, that the source is small in comparison to the wavelength. [21] [24] The time scale for the flow noise generation is $T \propto \frac{l}{u}$. l is the characteristics length of the sound source. For example, for a flow duct, this would be the diameter of the duct. With that the proportion to the frequency is $f = \frac{1}{T} \propto \frac{u}{l}$. From the frequency the wavelength λ can be concluded as $\lambda = \frac{c}{f} \propto \frac{l}{Ma}$. The relation between the source region and the Mach number can be derived from $\frac{l}{\lambda} \propto Ma$. [24]

The sound produced by a monople noise source can generally describe flow noise due to unsteady mass injection into a resting medium. [17] The generated sound is dependent on the unsteady volume flow and the density of the medium at rest. [24]

There is a possibility to calculate the sound power radiated from a source, when the flow condition changes. They are called scaling laws. [21]
For the monople sound source, the scaling law is presented for the case of a fluctuating volume flow from a pipe outlet. The sound power W_M can be calculated from the mean unsteady volume flow Q, the density of the surrounding fluid ρ and the speed of sound c. [24]

$$W_M = \frac{\rho Q^2}{4\pi c} \tag{4.3}$$

The unsteady volume flow Q can be calculated from the volume velocity u and the diameter of the pipe d.

$$Q \propto ud^2 \tag{4.4}$$

The scaled sound power can be calculated by the following equation with the frequency f, describing the periodicity of the tested process, for example of an engine or fan:

$$W_M \propto \frac{\rho f^2 u^2 d^4}{c} \tag{4.5}$$

Dipole sources can be used to model for example loudspeakers in free field, when the wavelength exceeds the loudspeaker diameter. Furthermore, fixed solid objects in a flow generate noise like a dipole source. [24]

At an object flow gets separated, which leads to a separation point and a turbulent wake region behind the object, where force fluctuations generated vortexes. This is described in vortex shedding, which generates sound. [21] The acoustic energy gets coupled to the kinetic energy of the vortex. The acoustic energy then gets dissipated downstream. [24]
This is also shown in figure 4.4. Lighthill´s theory was extended in Curles´s theory to describe this further.

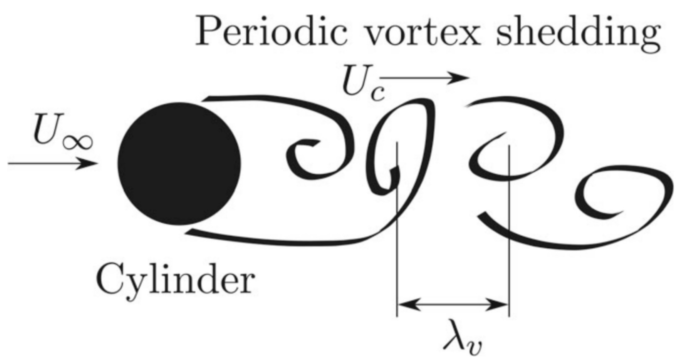

Figure 4.4: Vortex shedding [17]

Another application for flow acoustic noise sources are propellers and fans. They generate harmonic noise, which can be described by the BPF. [21]

$$BPF = \frac{number\ of\ blades}{rotational\ frequency} \tag{4.6}$$

So, dipole source can be used to model unsteady external forces or pressure, which are acting on the surface of a solid object in the flow. [17]

The sound power of a dipole source W_D is calculated from the mean total fluctuating force F, which acts upon the fluid, the density ρ and the speed of sound of the medium c.

$$W_D = \frac{F^2}{12\pi\rho c^3} \tag{4.7}$$

The varying force F for the case of a pipe opening, can be scaled by the mean flow velocity u and the diameter of the pipe d.

$$F \propto \rho u^2 d^2 \tag{4.8}$$

From that the scaling law for dipole source can be derived, with f being the frequency, describing the periodicity of the process, for example of an engine or fan. [24]

$$W_D \propto \frac{\rho f^2 u^4 d^4}{c^3} \tag{4.9}$$

The quadropole source, which was already mentioned, is correlated to sound from free turbulence [24]. An example for that is for example jet noise for high Ma [21].

There are more dimensionless aeroacoustic parameters then just the Mach number, which was already presented in equation 4.2. There also is the Strouhal number St, which gives an indication about the scale of periodic noise in turbulent flow and is calculated from the Strouhal frequency f_{St}, the characteristic length l and the mean flow speed u. [24]

$$St = \frac{2\pi f_{St} l}{u} \tag{4.10}$$

The Strouhal frequency f_{St} can be calculated represents the harmonic component of the system under investigation. For a flow it is calculated from the mean flow velocity u and the characteristic length L for the sound source under investigation [21]:

$$f_{St} = \frac{u}{l} \tag{4.11}$$

This can be, for example, the outlet diameter of a pipe or the size of an object in the flow. The Strouhal frequency gives an indication on the "characteristic frequency of the flow generated sound". With a flow fan it is the BPF. [21]

And there is the Helmholtz number He, which indicates the "size of the source region" and whether is can be regarded as compact. [21] For that the source or the characteristic length l of the system is compared to the wavelength λ. If $k \cdot l \ll 1$, the source is compact. [17] The Helmholtz number is dependent on the St and Ma. [21] [24]

$$He = St \cdot Ma = \frac{2\pi f_{St} l}{u} \cdot \frac{u}{c} = \frac{2\pi f_{St} l}{c} = k \cdot l = \frac{2\pi l}{\lambda} \tag{4.12}$$

4.1.2 Fan Noise

Axial flow fans are generally used to move a medium with a certain pressure. In a duct, the flow fan running at a certain rotational speed creates a pressure, so that the air gets sucked into the duct.

4.1.2.1 Fan Scaling Laws

Typically the performance of a fan is displayed by plotting the static pressure, absorbed power or the fan efficiency against the flow rate under certain operation conditions. Guide vanes behind an axial fan, like they are in the Epiroc silencer, can increase the pressure and the efficiency. From the fan performance parameters, the affinity or fan scaling laws were derived. They can be used to determine the performance parameters from a known fan 1 to an unknown fan 2, which differs from fan 1 in the fan size D_2.

$$Q_2 = Q_1 \times \frac{N_2}{N_1} \times \frac{D_2}{D_1}^3 \tag{4.13}$$

$$p_2 = p_1 \times \frac{N_2}{N_1}^2 \times \frac{D_2}{D_1}^2 \tag{4.14}$$

$$P_2 = P_1 \times \frac{N_2}{N_1}^3 \times \frac{D_2}{D_1}^5 \tag{4.15}$$

Here D_1 and N_1 represent the fan size in m and the fan speed in revolutions per second of the fan with the known performance parameters. The volume flow Q in $\frac{\mathrm{m}^3}{\mathrm{s}}$, the total pressure p in $\frac{\mathrm{N}}{\mathrm{m}^2}$ and the absorbed power P in W can be calculated for fan 2 from the performance parameters of fan 1. [31]

4.1.2.2 Noise Generation around Fans

Figure 4.5 gives an overview on the sound generated by flow fans. When looking at the frequency spectrum of a fan, the fan noise consists of broadband noise and strong frequency peaks.
In the chart the noise radiated from a flow fan is categorised by its source type.

The first on the left is the monople sound source. Blade thickness noise is radiated like a monopole sound source. It describes the sound generated from displacing the surrounding medium at rest through the rotating blades. For a fan, thickness noise goes back to the periodic blade passing in the medium, which leads to sinusoidal pressure variations. [31] In [17] it is described further, that the noise is dependent on the speed of the fan or propeller. The noise generation is stronger with higher fan speed because the displacement of the medium increases.

The sound radiated like a dipole source is divided into noise induced from steady rotating and unsteady rotating forces.
The noise generated by rotating forces is called Gutin Noise and occurs in uniform stationary flow. The rotating forces act on the moving fan blades and cause periodic pressure fluctuations. Usually Gutin noise is important, when handling high Mach number flows. [11]

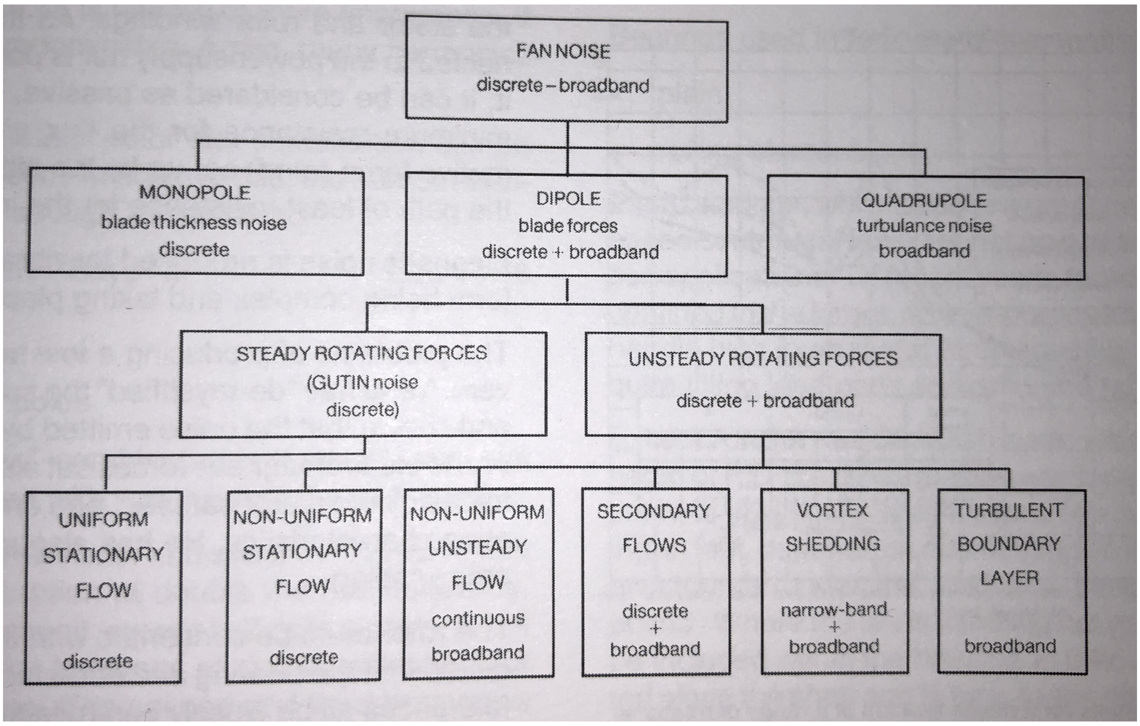

Figure 4.5: Overview of Fan Noise [31]

The other category on the chart for dipoles sources is about noise from unsteady rotating forces, which act on the fan. There are a number of further noise mechanism categories, which lead to periodic and broadband noise.
The BPF goes back to the first box, non-uniform stationary flow. The BPF can be affected by the guide vanes. [11] The size of the gap between the fan and the guiding vanes and the numbers of blades of the fan and the guide vanes affect the generation of the harmonic noise. [31]
The field of non-uniform unsteady flow describes the sound generated by turbulence on the inlet of the fan. These turbulence generate low frequency broad band noise. [11]

The categories "Secondary Flow", "Vortex Shedding" and "Turbulent Boundary Layer" can be summarized under self-noise according to [11]. Here sound generated from the interaction between the flow and the blade is described.

The category "Vortex Shedding" describes noise, which is generated by the flow separation at the blade. [31] Another important contributor to the sound field, is the tip clearance noise. It raises the noise level in the high frequency range. Tip clearance noise goes back to vortexes, which are generated, when the air moves through the tip clearance from a high to a low pressure region. [11]

The last source category is the quadrupole sound source. The broadband noise goes back to the turbulence in the flow, which were described in 4.1.1, or vortex noise.

Noise generation due to flow interaction at edges and generation of vortexes also occurs on the trailing and leading edge of an airfoil and on the blade tips. [23][17] They will be described further below.

Trailing and leading edge noise originates from the interaction of the turbulent field with the airfoil edge. The mechanism is shown in figure 4.6. Leading edge noise is generated from eddies in the upstream turbulent field. The varying velocity in the turbulent region creates pressure fluctuation on the surface of the foil. This results in unsteady lift, which generates the noise. The directivity of the noise radiation is dependent on the size of the eddies and the chord of the propeller or fan. For low frequencies, where the size of the eddy is bigger than the chord, the sound is radiated in a dipole pattern. For the high frequency case, with the eddies being smaller than the chord, the directivity is of cardioid character. [17]

There are two types of trailing edge noise. There is a broadband noise component, which goes back to the unsteady flow interacting with the trailing edge, see figure 4.6. At the edge the turbulent field experiences an impedance change, which leads to diffraction of the pressure-field. But at the trailing edge also a tonal noise can be generated. This could go back to vortex shedding at a blunt trailing edge or a feedback loop between the turbulent boundary layer and the acoustic waves. This noise generation behind this noise component is still part of research and not fully understood yet. [17]

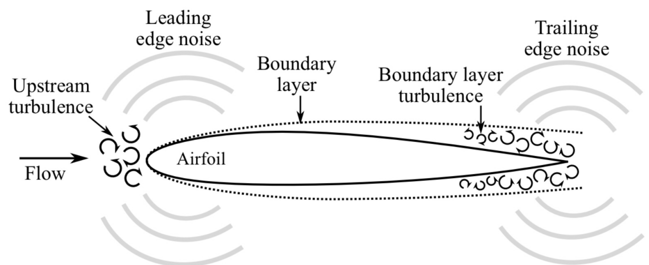

Figure 4.6: Leading and trailing edge noise [17]

4.1.2.3 Sound from Fans in Ducts

When an axial flow fan is placed in a duct, it can be described by a dipole sound source below the cut-off frequency for plane waves. [24]
In [17] a model is described to determine sound radiation from a dipole source in a duct, which is the theoretical case for a propeller or fan in a duct. From the model it can be concluded, that the radiated sound power at low frequencies from a fan placed far away from the end of a finite unflanged duct is 6 times stronger than from a free dipole source. For a flanged duct the the sound power increases by a factor 3, when the fan is built into a duct. For higher frequency many modes in the duct are excited and the sound radiation from the fan in the duct goes more and more towards the radiation of the fan in free-field. A more direct radiation adds to the sound power if the source or fan is positioned close to the end of the duct as well as scattering modes.

The blade passing generates periodic pressure fluctuations in the form of supersonic spinning modes. Flow separation at objects like guide vanes increases the sound generation coming from supersonic spinning modes. The Tyler-Sofrin rules suggests to choose the following ratio $number\ of\ guiding\ vanes \geq 2 \times number\ of\ blades$ to avoid supersonic modes, which contribute to the BPF. [24]

4.2 Sound Propagation in Ducts

In the following, the sound propagation of waves in ducts is described. The topic will be important for the interpretation of the measurement results of the scale model duct and the simulation model. Here, the duct alone will be investigated and with silencing treatment. Also, a fan in a duct excites the duct's modes. The simulation will also focus on plane waves in the duct, which will be discussed here.,

Low frequencies in a duct propagate as plane waves. Their sound pressure distribution over the cross-section is constant and fluctuates only along the duct length. The region of plane wave propagation is usually limited to where half the wavelength is bigger than the diameter of the duct.

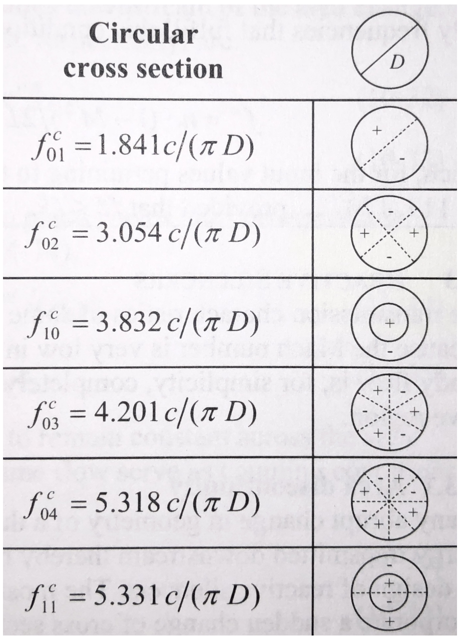

Circular cross section	
$f_{01}^c = 1.841\, c/(\pi D)$	
$f_{02}^c = 3.054\, c/(\pi D)$	
$f_{10}^c = 3.832\, c/(\pi D)$	
$f_{03}^c = 4.201\, c/(\pi D)$	
$f_{04}^c = 5.318\, c/(\pi D)$	
$f_{11}^c = 5.331\, c/(\pi D)$	

Figure 4.7: Equation of the cut-on frequency for different mode shapes [21]

Modes can propagate in the duct with increasing frequency. Every mode has a so-called "cut-on" frequency. Below the cut-on frequency the mode will be damped strongly and can not propagate. With increasing frequency also an increasing number of modes can propagate through the duct. For the plane wave the sound pressure does not fluctuate over the cross-section. This is different for the modes, with increasing frequency the fluctuation over the cross-section area of the duct increases. This can be observed in figure 4.7 on the right side of the table. On the left side,

the formulas for calculating the cut-on frequency for the different mode shapes is displayed. The frequency is calculated from the duct diameter D and the speed of sound c. The number values, which differ for every mode shape, can be derived from the Bessel function. The equation for the 01-mode gives the cut-on frequency for that mode, but also is the cut-off frequency for the plane waves being able to propagate in the duct. [21]
The modes in a duct are orthogonal, so their sum can describe the entire pressure field. [17]

When plane waves propagate in a duct, they do not have a change in their amplitude along the propagation path. This can be derived from modeling a piston at the end of a pipe. At the position x=0, where the piston is attached to the duct, the velocity of the piston U must be equal to the velocity of the pressure field in the duct u.

$$u = U \tag{4.16}$$

The wave induced by the piston can be described by the solution of the one-dimensional wave equation. The wave equation is

$$\frac{1}{c^2}\frac{\partial^2 p}{\partial t^2} - \frac{\partial^2 p}{\partial x^2} = 0 \tag{4.17}$$

And the general solution is

$$p(x,t) = f(x - c/t) + g(x + c/t) \tag{4.18}$$

which describes a wave propagating in positive and a wave propagating in negative x-direction. For the piston, there is a wave traveling in the positive x-direction $f(x - c/t)$. From the pressure p the velocity can be calculated since the pressure and the velocity u are connected by the density ρ and the speed of sound c.

$$p = \rho c u \tag{4.19}$$

To conclude, the pressure in the duct can be described by

$$p = \rho c U(t - x/c) \tag{4.20}$$

From this it can be concluded, that their is no transmission loss in the duct for plane wave propagation. [10]

4.2.1 Breakin and Breakout Noise

Sound transmission from the inside of the duct to the outside through the duct wall is described by breakout noise. Noise from the environment, which enter the pressure field in the inside of the duct over the duct wall by causing vibrations is breakin noise.
In figure 4.8 a typical transmission curve for breakin noise is displayed.

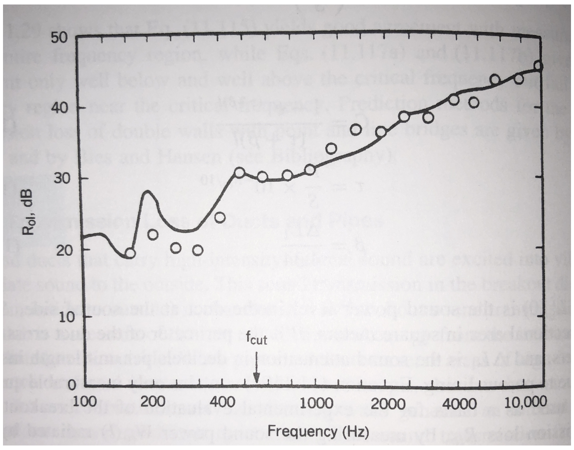

Figure 4.8: The breakin sound transmission loss from a rectangular metal duct: solid line describes measurement result and the points show predicted values [22]

4.3 Noise Mitigation Measures

Noise Mitigation measures to achieve sound reduction can be divided into primary and secondary measures. Primary measures aim for achieving the noise reduction by improving the sound source of the noise.
If there can be no further optimisation of the source, secondary measures can be applied to the object in question to get a further decrease in the emitted sound level.

Some of the possibilities, which can be applied to a fan to reduce its noise, were already presented in section 3. Possibilities mentioned there, were amongst others to put serrations on the blade edges, apply irregular spacing between the blades or putting porous material on the blades.

Also ideas on different kinds of secondary measures where presented in section 3. The use of silencers with new absorptive materials like MPP or AM were mentioned.

4.3.1 Reactive and Resistive Silencer

Generally there are two types of silencer types. There are reactive silencers and resistive silencers. The main difference is that the reactive silencers achieves sound reduction by reflecting part of the sound energy through an impedance change, while the resistive silencers transform the acoustic energy into heat to reduce the sound. [21]

There are a few different applications on reactive silencers for flow ducts. A jump in the cross-section of the flow duct leads to a change in the impedance, so that a small amount of sound energy reflects back into the opposite propagation direction, which reduces the acoustic energy, that propagates further along the propagation path. This mechanism is also applied to expansion chambers. Here the propagating

wave is reflected at the jump from the small to the bigger cross-section and again at the second jump from the bigger to the smaller cross-section of the duct.
Then there are different applications, which all go back to having a side branch to a duct system. There is the quarter wavelength resonator or the Helmholtz resonator. The quarter wavelength resonator is a duct attached to the main duct like a side branch. The length of this silencer can be fitted to a certain quarter wavelength to gain the most reduction for a certain frequency and its odd multiples. The Helmholtz resonator is another side branch application. It consists of an enclosed volume and that volume is connected to a smaller duct, which is connected to the flow duct. The Helmholtz resonators are like a mechanical mass-spring system and are most responsive to their resonance frequency.

The transformation from acoustic energy to heat is achieved by porous materials. This absorption material can for example be lined on the walls of a ventilation duct. [21]

4.3.2 Transmission and Insertion Loss

The properties of silencers are usually stated by the sound transmission loss (TL) or the sound insertion loss (IL).

The TL is defined as the difference of the sound power that incides on a test object W_{in} and the sound power that gets transmitted W_{tr} through the test object [7]:

$$TL = 10 \log_{10} \frac{W_{in}}{W_{tr}} \tag{4.21}$$

The IL is also used to describe the properties of a silencer. Instead of giving the difference between the incident and transmitted sound power, the IL indicates the effect by adding a silencer to a system. It is calculated from the sound power of a system with the silencer inserted W_I and without the silencer W_0. The sound power is observed at the same point behind the silencer. For the TL the power in front and behind the test object is observed. [22]

$$IL = 10 \log_{10} \frac{W_{wo}}{W_{w}} \tag{4.22}$$

In figure 4.9 the typical TL of a single wall is displayed. Different regions are marked in the plot. In the plane wave region, the TL is determined by the stiffness of the wall material. Then the first resonances of the wall lead to peaks and dips in the TL in the few-mode-region. Above the TL is determined by the mass of the wall. The TL increases with 6 dB per octave band. There is another resonance dip at the critical frequency f_c. [21].

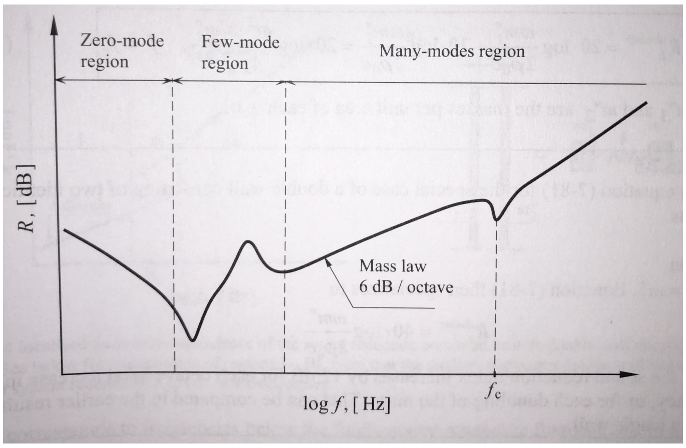

Figure 4.9: Typical reduction curve of a single wall [21]

4.3.3 Silencer under flow conditions

The absorbing properties of a silencer change, when flow is introduced to a system under investigation. In figure 4.10 it is displayed. The system investigated in figure 4.10 is a straight duct with a Helmholtz resonator. Without flow, the resonance frequency of the silencer is around 400 Hz, so that the highest TL is achieved there. When flow is added to the duct, the characteristics of the TL change. With a low flow velocity (Ma=0.1) the frequency peak in the TL shifts toward higher frequency. With even higher flow velocity (Ma=0.2), the TL decreases strongly. And the peak in the curve becomes much broader.

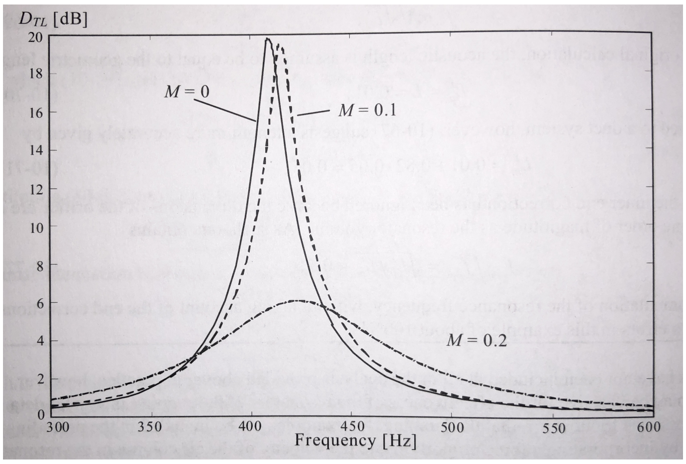

Figure 4.10: The TL for a Helmholtz resonator on a duct changes with different flow velocities[21]

4.3.4 Round Silencer

For round ventilation ducts round silencers are used. They have an advantage in the reduction of low frequency noise. Their higher stiffness due to the round duct wall leads to a higher TL of the silencer. The most common setup of round silencers is with absorptive porous material lined on the silencer duct wall. In the following figures, the silencer is divided by the passage and the liner. The diameter of the passage is described by $2h$, while the thickness of the porous layer is described by d. The figures show the normalized sound attenuation L_h for an incident from normal direction, which is dependent on the geometry and the propagation constant Γ_c.

$$L_h = 8.68hRe\{\Gamma_c\} \tag{4.23}$$

Γ_c is the propagation constant of the coupled wave, which propagates in the passage and the absorber. It is dependent on the impedance ρc of the fluid, the impedance Z_a, the propagation constant Γ_a of the porous material and the geometry. Usually Z_a and Γ_a are estimated by empirical equations. For those only the flow resistivity R_1 of the porous material needs to be known.
In figure 4.11 the computed normalized attenuation L_h for a round silencer is plotted against the normalized frequency $\eta = \frac{2hf}{c}$. The round silencer has a "liner thickness to passage ratio" of 0.5 and the plot show the attenuation level for different normalized flow resistivity values. The normalized flow resistivity was calculated by the thickness of the liner d, the flow resistivity R_1, the density ρ and the speed of sound c for the fluid material.

$$R = \frac{R_1 d}{\rho c} \tag{4.24}$$

In figure 4.11 it can be observed, that the attenuation increases to a maximum, when the diameter of the passage is equal to the wavelength. When the frequency increases further, the attenuation of the silencer decreases.

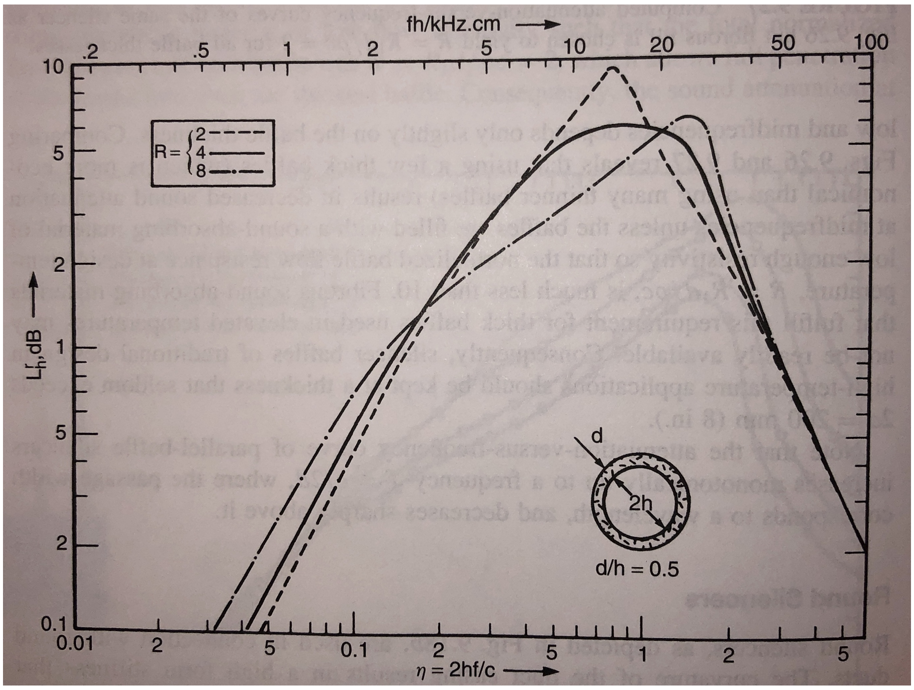

Figure 4.11: Computed normalized attenuation L_h over normalized frequency η for round silencer with a thickness-passage-ratio of 0.5 for different normalised flow resistivity values [22]

In figure 4.12 three cases are compared. The plot shows the noise attenuation of a round silencer without a center body, with a center body and with an absorbing center body. Usually round silencer have poor TL, when the passage is big compared to the wavelength. With a centered body in the passage, the passage is decreased and the sound reduction will increase until the wavelength fits the new passage.

In figure 4.12 it can be observed, that with each case, the sound attenuation increases strongly for higher frequencies. The frequency peak shifts towards higher frequency and the overall reduction in the higher frequency range increases as well.

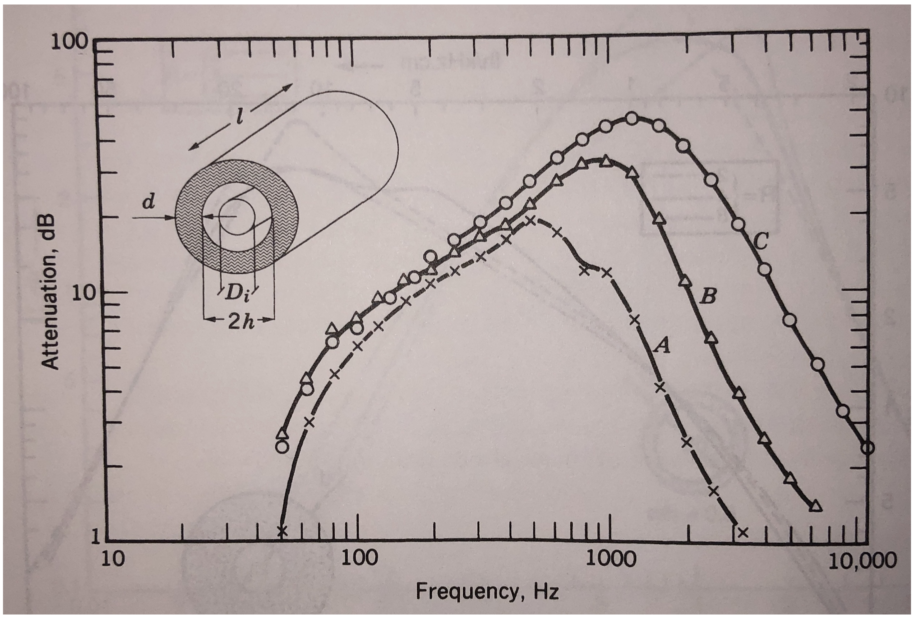

Figure 4.12: Computed noise attenuation for A. no center body, B. rigid center body and C. absorbing center body [22]

In figure 4.13 the behaviour of the round silencer is displayed with and without flow. There are two plots displayed. In the upper plot, the sound and the flow propagate in the same direction. In the lower plot, the sound and the flow travel in opposite directions.
The flow in the system changes the speed of sound.
When the flow and the sound propagate in the same direction, the attenuation of the low frequency components reduces with increasing Mach number or else flow velocity. The flow causes a velocity gradient, which in this case leads to the refraction of sound towards the absorber. In the high frequency range, the attenuation increases with increasing Mach number. But the increase is rather small.
In the second plot, the sound and the flow travel into opposite direction. Now the speed of sound decreases, which leads to an increase of the attenuation, when flow is added to the system or the flow velocity is increased. At high frequencies the attenuation decreases because the velocity gradient leads the sound towards the center of the passage.
Besides the change in sound propagation time and the different velocity gradients,

the flow also increases the flow resistance. [22]

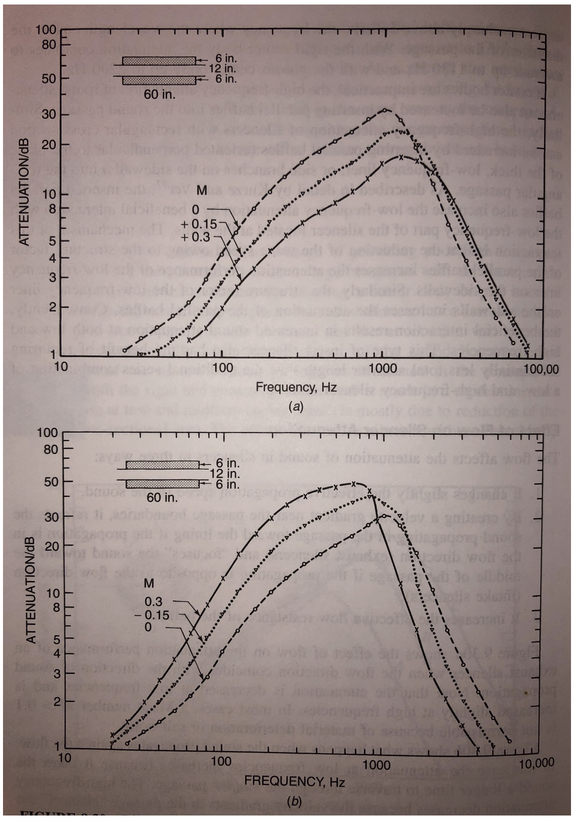

Figure 4.13: Attenuation of the round silencer with flow: (a) sound propagation in flow direction, (b) sound propagation against flow direction [22]

4.4 Fluid-Dynamic Scaling: Similitude

In this section, the scaling for fluid dynamic investigations is described. The aim for the design of the scale model is, that the fluid dynamics are comparable to the full-sized machine. But the requirements of the fluid-dynamic scaling have to be brought to agreement with the acoustic scaling and the material, that are available for building the scale model.
When scaling down a test object of an aerodynamic investigation, there are three so-called similarities, that have to be fulfilled.

The first is called geometric similarity. This one requires, that all linear dimensions are scaled down by the scale factor. An exception applies to angles. They have to be the same in the scale model as they are in reality. Another requirement is that the roughness of the surface is similar as well.

The second similarity aims to the kinematic properties. When the same position or point on the scale model and the full sized machine are compared, the flow has to move into the same direction at this point in both models and the magnitudes at this position has to be connected by the scale factor. So, the scale model also needs to have similar flow properties. If the flow of the test object is laminar, it should be the same for the scale model. The same applies for turbulent flow.

The dynamic similarity states, that at the same point on the scale model and on the test object the acting forces on a flow particle must come from the same direction and their magnitude should be scaled by the scaling factor. [13]

5

Design of the Scale Model

As described in section 1, the design of a scale model of the AVH90 ventilation system was conducted in the thesis project.

The use of a scale model for the experimental investigations gives a fast and efficient way to do measurements. Its easily available and cost-saving as it gives the possibility to test new noise mitigation measures in the model instead of directly applying them to the full-sized machine. In the scale model the noise reduction measure can be investigated on whether its effect is satisfying enough to built and test it on the full-sized machine as well. This approach can save time and costs.

The ventilation system Epiroc offers can be purchased in different sizes. The inner diameter ranges from 0.63 m to 2.24 m. The different products are scaled as well. For the product the scaling is focused on the fan. The acoustic treatment is the same for all product sizes. With this, design decisions for the scale model can be derived and changes can be investigated.

Due to practicality the scale model was built from available material. With the fan scaling laws and similarity requirements, the expected fan performance and flow parameters were calculated for the scale model. A short flow simulation was solved for the silencer in order to visualize the velocity and pressure field.

With the limited time in the thesis project only a scale model of the silencer was achieved. The scale model does not yet include the fan and guide vanes.

5.1 The scale model

For the scale model a 1.3 m long steel ventilation duct was used with a diameter of 0.63 m. It was decided to work with a bigger pipe because the larger diameter makes it easier to built inside the duct.

1.2 m, which is the silencer length of the AVH90 ventilation system, of the duct were layered with absorptive fiber material. The absorption material consists of pressed polyester fibers with a non-woven surface. It has a density of 25 kg/m^3. On top of the absorber a 1 mm thick perforated steel plate with 5 mm perforations and 3 mm spacing was placed. The last 10 cm, that were not covered with the absorber material, were left free intentionally to later insert the fan. Photos are shown in figure

5.1. The perforated plate could be inserted into the duct separately. Also, just 1 m of the absorber was covered with the plate for now.

In table 5.1 below, the dimensions of the AVH90 and the resulting dimensions for the model duct are listed. The full-sized dimensions are taken from a CAD model or were calculated from the given geometries.

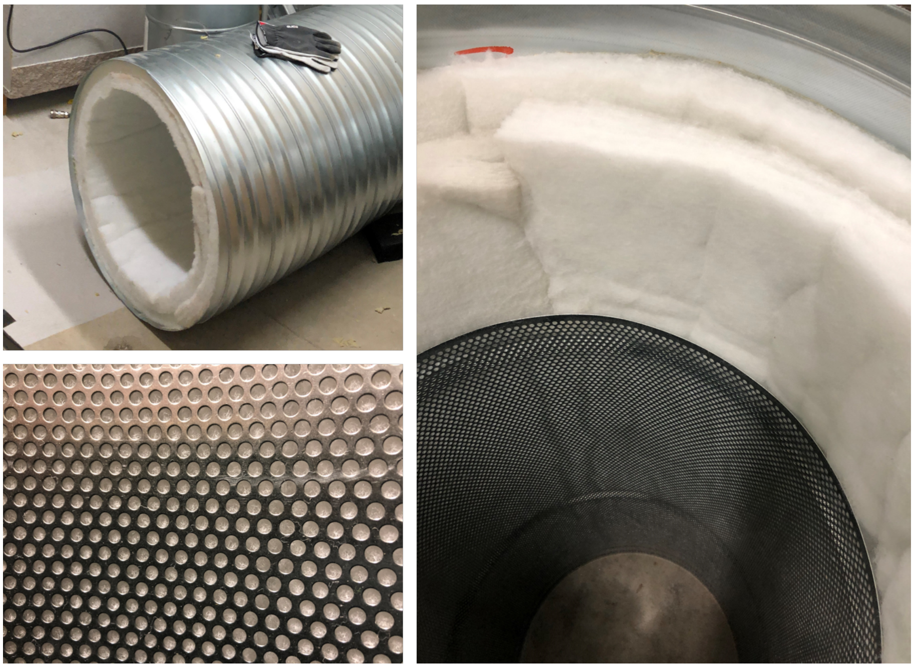

Figure 5.1: The scale model of the silencer

Table 5.1: The dimensions of the AVH90 ventilation system and the scale model

	ventilation system	scale model
outer duct diameter	1.042 m	0.63 m
silencer length	1.2 m	1.2 m
cavity with absorption	70 mm	70 mm
perforated plate		
- thickness	1 mm	1 mm
- hole diameter	5 mm	5 mm
- spacing	3 mm	3 mm
remaining inner duct diameter	0.9 m	0.488 m
blade length	168 mm	91 mm
tip clearance	2 mm	2 mm
hub diameter	560 mm	302 mm

Not all dimensions were changed. The depth of the absorption layer and the dimensions of the perforated plate were kept the same. Because the acoustic measure in the product line is not adapted to the size, the acoustic measure in the scale model was not changed. This gives the opportunity to investigate the behaviour of the silencer and the influence of the absorber and the perforated plate further.

For the AVH90 some effect by the absorber and the perforations could be seen in figures 2.5 or 2.6 and 2.11. From the sound pressure level measured under flow conditions a reduction due to the absorber could be observed above 160 Hz. And a strong influence by the perforation at 400 Hz.
It has not been studied closer yet how the dimensions of the cavity and the perforations influence the absorption in regard to the frequency, but with the same acoustic treatment in the scale model as in the AVH90 it is possible.
The acoustic properties of the silencer are strongly dependent on the geometries. The depth of the absorption layer and the size of the perforation holes are crucial to its absorption properties over frequency. The scaling of those geometries by the scaling factor would lead to different absorption properties between the scale model and the full-sized silencer.
With adding the same acoustic measure into the scale model, it is easier to conduct this comparison and to find out more about the silencer. It could be expected that the acoustic treatment has a similar behaviour over frequency. Its also interesting to see how the behaviour of the absorber might change in dependency to the size of the flow duct.
From the results, the effect of the acoustic treatment on the other machines could be derived and one can find out whether it is useful to fit the acoustic treatment to the machine size in the future to gain further noise reduction.

So, the parts of the silencer -the size of the cavity and the perforated plate- were kept the same for the scale model, to be able to have the absorbing effect as close as possible between both models.
With that, only the inner duct diameter changes from 0.9 m to 0.488 m, so the scaling factor is 1.84.

The absorption material of course defines the behaviour of the silencer as well. The glass wool material they have on the ventilation system was replaced in the scale model by a 7 cm layer of polyester fiber material.

Another parameter, which was not scaled down, was the length of the silencer. By the scaling factor, the length should have been 0.65 m. The expectation was, that the length would only add to the absorptive performance of the scale model. So the TL would be higher, due to a longer absorption area.

Furthermore, the size of the tip clearance, the space between the blade and the duct, was kept at 2 mm and for that the hub diameter was reduced by 2 mm. This changes the scale factor for the fan diameter from 1.84 to 1.85. But regarding construction it will be easier to have more room for maneuvering.

From the aerodynamic point of view and the geometric similarity law, all the dimensions of the scale model should have been scaled by 1.84. But since the scaling was first and for-most done from an acoustic point of view, the aerodynamic requirement was not applied fully. As explained, this would have changed the properties of the silencer regarding the absorption properties. But the dimensions, which are flow dominated, in this case the inner duct, where the flow propagates, and also the fan can be scaled by this factor. A slight change is there due to the size of the tip clearance. The influence on the flow and fan parameters has to be investigated, so one can see how much dynamic and kinematic similarities are fulfilled. Another aspect here is also the length of the duct. With the longer length, the points between the scale and the full-sized ventilation system change only in two dimensions. What this means for the flow regime and the forces applied to the system by the fan blades needs to be investigated in the future.

5.2 The expected Flow Properties and Fan Performance

The predicted fan performance and flow properties are listed in table 5.2. The reference values were taken from the performance curves from the Epiroc AVH90 and the measurement case presented in chapter 2 to be able to compare the scale model to those measurement results in the end. The calculated fan performance values are only valid, if the scaled fan has the same surface structure and blade angle.

Table 5.2: The performance parameter and flow properties of the AVH90 ventilation system and the scale model

	AVH90 measurement section 2	scale model
blade angle	44°	44°
fan speed	3000 rpm	1500 rpm
fan diameter	0.896 m	0.484 m
flow rate	$20.5\,\mathrm{m^3/s}$	$1.62\,\mathrm{m^3/s}$
fan power	31.8 kW	0.18 kW
pressure	1300 Pa	94.83 Pa
BPF	400 Hz	200 Hz
flow velocity	50.65 m/s	46.18 m/s
- area of the cross-section	$0.64\,\mathrm{m^2}$	$0.19\,\mathrm{m^2}$
Mach number	0.15	0.13
Reynolds number	$2.99 * 10^6$	$1.48 * 10^6$
Strouhals number	44.66	13.28
Helmholtz number	6.59	1.79

The measurements were conducted with the blade angle of 44° and with a fan speed of 3000 rpm. The available fan engine for the scale model is limited to 1500 rpm, that is why the scaled values were calculated for 1500 rpm. From the data sheet of the AVH90, it is known, that the performance depends on the blade angle, so the installation in the scale model either needs adjustable fan blades like in the AVH90 or needs to represent a fixed operating point. For the calculation and for comparability to the provided acoustic results from section 2, the fan scaling laws were applied to the performance parameter of the 44° blade angle.

The performance parameters in table 5.2, where calculated following equations 4.13, 4.14 and 4.15. It can be observed, that due to the change in the diameter and the fan speed, the flow rate, pressure and power become much lower.

The rotational speed is expected to be different in the scale model, which means, that the BPF will shift. With the usual number of 8 blades, the scale model cannot represent the same BPF as the ventilation system. If it turns out, that the silencer is most absorbing around 400 Hz and new countermeasures targeting that frequency are of interest, the blade number on the fan needs to be adjusted from 8 to 16 in order to get the same resonance peak and harmonics in the spectra of the scaled fan. Another way is to use a different motor, so that the fan can be operated at 50 Hz. And a last possibility is to scale the acoustic treatment to absorb the BPF of the scale model. Then countermeasures targeting 200 Hz can be tested in the scale model and then they can be scaled to absorb 400 Hz in the AVH90.

For the aeroacoustic parameters, the flow velocity was calculated from the flow rate and the area of the duct opening. They differ by 4 m/s.
With the flow velocity the dimensionless numbers were calculated in order to make conclusions regarding the kinematic similarity. It can be seen, that the Mach number is low and the difference between the values is rather small. The Reynolds number shows, that the flow in the AVH90 is more turbulent than in the scale model.
The Strouhal and Helmholtz number can give an indication of the comparability of the acoustic source. The Strouhal number was calculated with the flow dominating frequency as the BPF, following equations 4.6 and 4.10. And the Helmholtz number was calculated from equation 4.12. The results show differences between the values. The higher Strouhal number gives an indication that the harmonic oscillation will be more dominate in the flow of the ventilation system than in the scale model. Consequently the Helmholtz number decreases as well.

In conclusion this means, that the ventilation scaled in the way described in table 5.2 has a slight difference in its kinematic properties due to the lower velocity. The difference in its acoustic properties is stronger due to the position of the BPF. This can be improved by adjusting the number of blades on the fan from 8 to 16 in case the rotational speed cannot be increased.

5.3 Flow Study

A CFD study was conducted in Comsol Multiphysics 6.1 on a 2D model of a silencer part. This was conducted for the silencer with and without a body obstructing the flow.

5.3.1 The Geometry of the Simulation Model

The simulation model was not solved for the entire geometry in order to save computational time. The main interest was to see how the perforated plate interacts with the flow and how the model result changes with an object.

The 2D model was build out of a 0.2 m × 0.1 m rectangle. The perforations were built from an array of 0.005 m × 0.001 m rectangles along the length. And the cavity behind the perforated plate was modelled by a third rectangular with 0.2 m × 0.07 m. So, the dimensions of the silencing components were kept the same.

A simulation with a solid object in the flow was conducted to investigate the changes to the flow when placing the centrum-baffle into the silencer. A geometry similar to the shape of the baffle, built from a circle and a rectangle, was subtracted from the first rectangle.

The domain material, which was added to the geometry, was air. This kept the model simple, but the absorptive layer was neglected.

5.3.2 Setup of the Flow Study

For the flow study the Comsol physics model "Turbulent Flow, k-ϵ" was set up.

The "Turbulent k-ϵ" model is a good choice to do a first simple calculation. Compared to other models it does not rely on initial assumptions. Furthermore, computational resources can be reduced as it does not require a fine mesh. On the other hand it can not simulate flow close to walls. For that one has to include the wall function. But that does not calculate the buffer layer. [19]

The following details on the flow simulation and the Comsol applications used for the calculation can be found in [4].

In the "Turbulent Flow, k-ϵ " model "incompressible flow" is selected for the model, which applies a constant density in the fluid. The simulation model solves for the "Reynolds-averaged Navier Stokes" equation and "wall functions" are included to describe the flow close to wall boundaries.

Three nodes need to be added to the model.
A "Wall" node was included. Here "no slip" boundary conditions are included for the wall, which puts the velocity at the wall equal to zero. No wall roughness was applied to the model.
Then an "Inlet" and an "Outlet" node need to be applied together. At the inlet the flow velocity U_0 was added. The normal inflow velocity was set to 50 m/s. When the velocity is specified at the inlet, the pressure has to be set at the outlet. The relative pressure at the outlet boundary is set to zero. Also, the suppression of back-flow through the outlet boundary is added by default.

To solve the model a fluid dynamic physics-controlled mesh with an "extra fine" element size was applied to the model. It consists of 78979 domain and 2138 boundary elements. The smallest element size is 2.57×10^{-5} m. The maximum element size was 0.002 22 m. The resolution on the walls is higher. The decision on the "extra fine" mesh seemed a good compromise between the resolution around the perforations and the computational time.

5.3.3 Simulation Results

In figure 5.2 the geometry, which was described in section 5.3.1, of the simulation model can be observed. Generally one can say, that the geometry consists of three parts. The upper rectangle, which is green in figure 5.2a, is the flow duct. The inlet is on the left side and the flow travels with 50 m/s to the outlet on the right. The upper boundary is solid. The lower boundary is perforated. The thin perforation layer can be observed, for example, in figure 5.2c. Here the perforated plate from figure 5.2a is shown enlarged. And the third part, which is blue in figure 5.2a, is the 7 cm cavity, which is on the silencer.

Two cases were simulated. In figure 5.2 the results of the silencer without an object in the flow duct are displayed. In figure 5.3 the simulation results for the flow duct with the object are shown. The model was solved for the velocity field and the pressure distribution. Both are displayed here. To display the calculation results better, streamlines were added to the velocity results. But for the stream lines on the individual perforations only the first was selected.

In figures 5.2a and 5.2c the flow velocity is displayed for the first simulation case without the object. In figure 5.2c the streamlines around the perforation holes are enlarged. In figure 5.2b the pressure distribution is shown and in figure 5.2c the perforations are displayed again. The range on the colorbar is fitted to the results shown in figure 5.3. As a consequence some of the smaller variations get lost. In order to show the pressure distribution better, figures 5.2e and 5.2f show the results with a smaller pressure value range.

From the result, shown in figure 5.2 of the simple silencer without the object it can be observed, that the flow entering the duct does not have any velocity or pressure fluctuations along the propagation path.

In figure 5.2a the air flow travels on straight paths through the duct with a constant speed. It can be observed, that there is a decrease in velocity in the close region towards the perforated plate, which can be described by a laminar sublayer. It increases slightly with the length of the duct. In the perforations and the cavity the velocity decreases strongly. Since the space is closed, the flow kind of swirls around. The cavity in the model is filled with air, but it can be expected, that in the real silencer, where the cavity is filled with absorber, the flow propagation is quickly reduced by the flow resistance of the material.

Two scales were added for the pressure. In figures 5.2b and 5.2d the scale is comparable to the pressure results in figure 5.3. In figures 5.2e and 5.2f the pressure range is smaller in order to show the pressure fluctuations better. When looking at the pressure field in figures 5.2e and 5.2f it can be observed, that the pressure decreases from the inlet to the outlet side. The pressure field looks different for the upper boundary of the model with just the smooth wall and the lower side, where the perforations are added. There are more fluctuations at the perforations. The edges show high pressure, while the hole is more of a low pressure region (see figure 5.2f.
When looking at figures 5.2b and 5.2d and comparing the result to figure 5.3, it can be seen, that the pressure fluctuations are rather small compared to the the second simulation case.

When adding the centrum-baffle as a solid object in the flow duct, the pressure and velocity vary much more. The results are shown in figure 5.3. In figures 5.3a and 5.3c the velocity in the flow duct and at the perforations are displayed. In figures 5.3b and 5.3d the pressure along the flow duct and at the perforations are shown.

The velocity in figure 5.3a enters the silencer with 50 m/s, but at the tip of the baffle the flow gets separated. There is an area of high pressure (see figure 5.3b) and low velocity at that point. The flow separation increases the velocity above and below the baffle. It can be observed, that below the baffle, where the perforated plate is, the velocity is lower than on the upper side of the baffle, where the flow propagates between two solid boundaries. Behind the baffle is a wake region with vortexes and low velocity.
The flow that enters the cavity through the perforations swirls around stronger than before. In the area of the separation, the flow that gets pushed through the perforations at a higher velocity than the flow entering at the continuous regions like at the beginning or below the baffle. With that higher velocity the flow in the cavity manages to even exits the cavity again at the end due to the outer solid wall. But also this phenomena will probably not occur in the same manner due to the flow resistivity of the absorbing material.

The pressure result in figure 5.3b shows some higher pressure fluctuations in the flow duct. The cavity has higher pressure than before in figure 5.2, but also no pressure fluctuations. Some high pressure regions occur where the flow hits an object or an edge. This can be seen on the rear edge of the perforation in figure 5.3d and on the upstream side of the baffle.

To conclude, the object in the flow duct causes flow separation, vortexes and turbulence, which lead to noise generation. When looking back at the ventilation system, some ideas can be derived from the simulation to possibly get noise reduction. From the measurement results in section 2, it is known, that the ventilation system radiates strongest from the inlet and outlet opening (see figure 2.9. When the ventilation system is set up at the entrance of a mine, the inlet side of the ventilation system radiates into the outer environment. In figure 2.3 the setup of the ventilation system was displayed. With the centrum-baffle and the fan motor on the inlet side, the flow gets disturbed, which leads to flow separation, vortexes and turbulence like it was shown in figure 5.3. A steady flow propagation like in figure 5.2 could help to minimise the noise generations on the inlet side. For that, the centrum-baffle in the inlet silencer could be removed and the fan motor could be placed behind the fan and guide vanes. Then the flow disturbances on the inlet side are reduced and possibly less noise radiates into the surrounding environment.

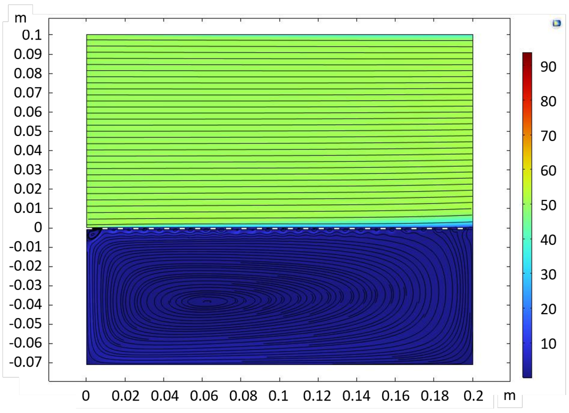

(a) Velocity field in m/s

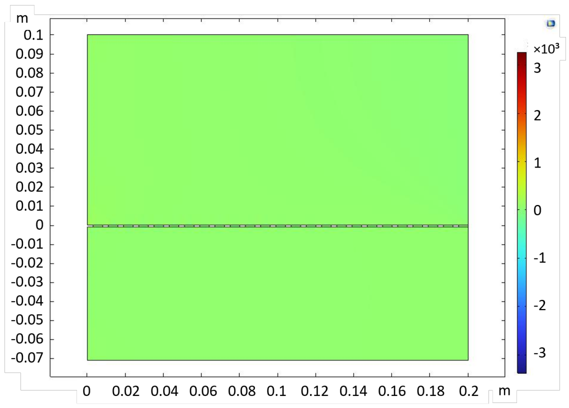

(b) Pressure distribution in Pa

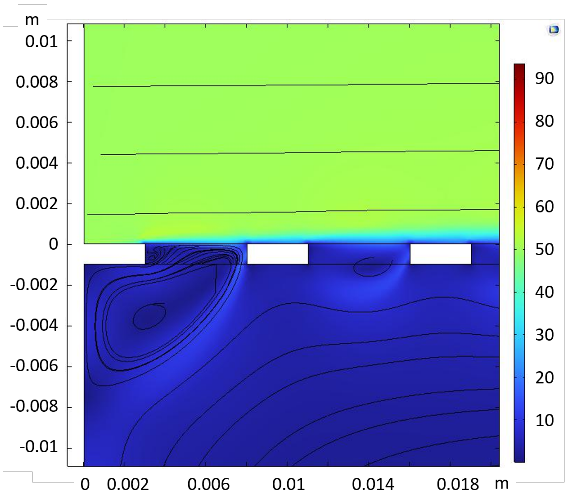

(c) Velocity field at the perforations in m/s

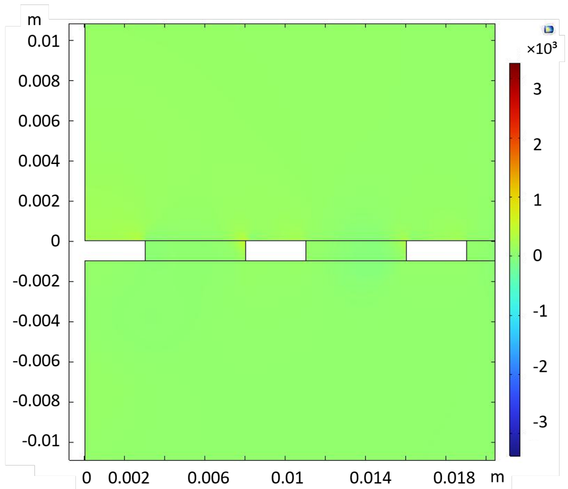

(d) Pressure distribution at the perforations in Pa

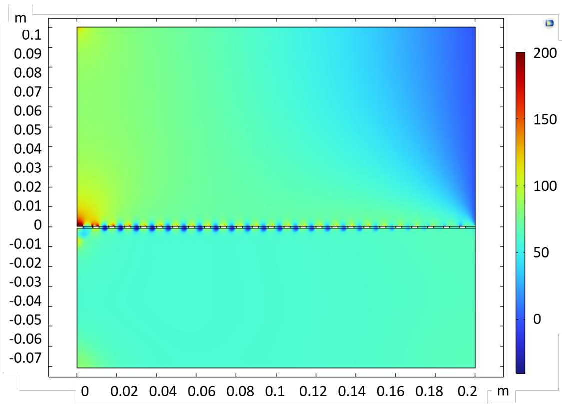

(e) Pressure distribution in Pa

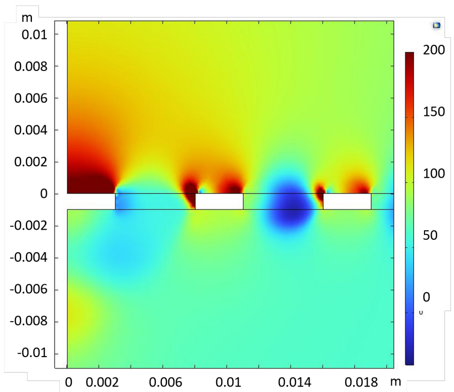

(f) Pressure distribution in Pa at the perforations in Pa

Figure 5.2: The pressure and velocity field of the silencer duct with an inlet flow velocity of 50 m/s

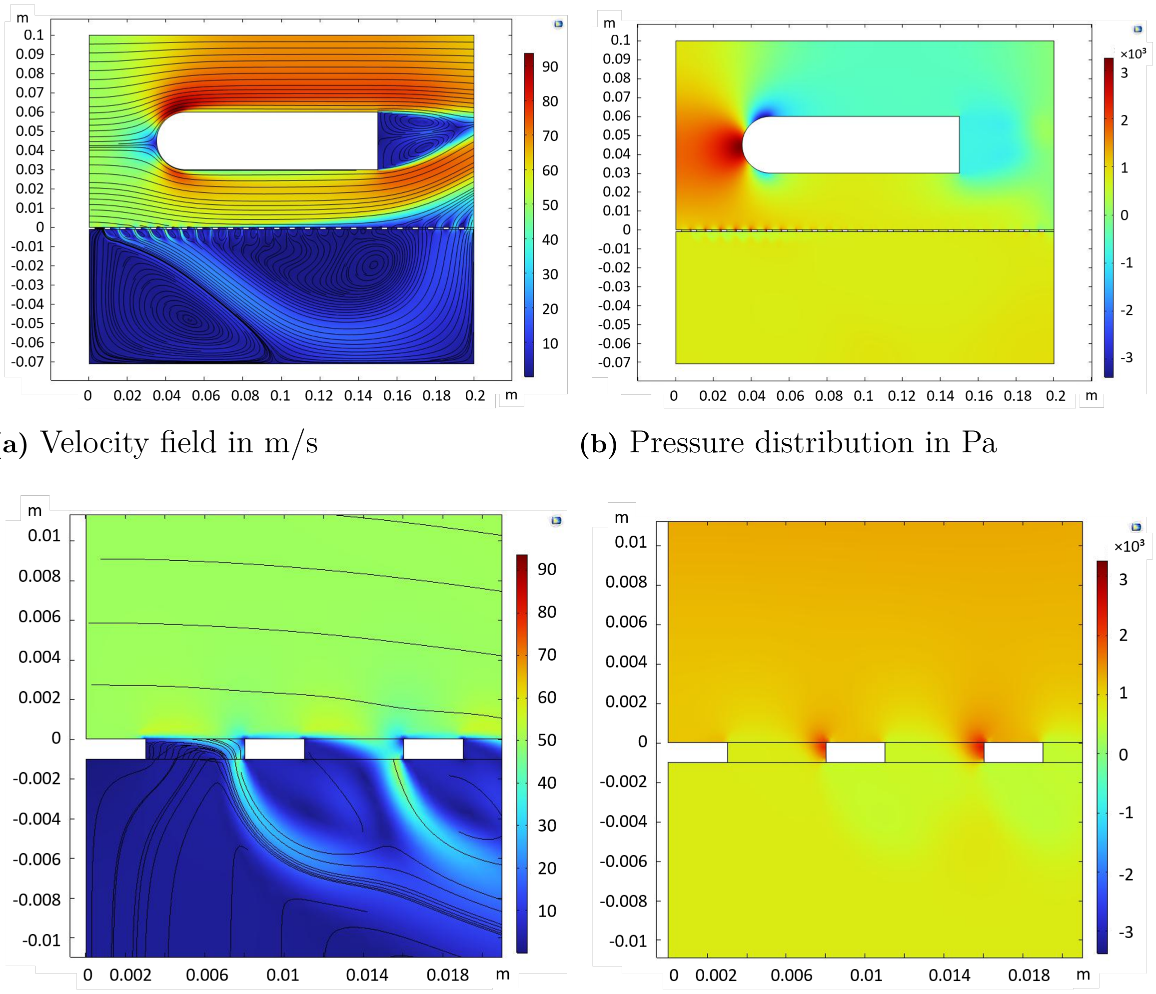

(a) Velocity field in m/s

(b) Pressure distribution in Pa

(c) Velocity field at the perforations in m/s

(d) Pressure distribution at the perforations in Pa

Figure 5.3: The pressure and velocity field of the silencer duct with the centrum-baffle in the flow with an inlet flow velocity of 50 m/s

6

Measurements with the Scale Model

In the following chapter the measurements on the scale model will be described. Two setups were tested. One for the determination of TL and a second setup to determine IL. The measurement setups and the procedure will be presented in detail. In the end, the measurement results will be discussed, which contain the investigation of the measurement environment and the results from the scaled silencer model.

6.1 Transmission Loss Measurements

To later investigate other noise mitigation measures, the acoustic properties of the scale model were determined with TL measurements using two rooms.

When determining the TL using two rooms the test object is installed in a window between two adjacent chambers. The source room (SR) is equipped with a loudspeaker source. In the so-called receiving room (RR), the sound pressure field is measured. From the level difference between the rooms and some correction factor, the loss due to the sound transmission through the object can be determined.
Two different measurement methods for determining the transmission loss were conducted.
The methods and the setup of their Testlab Software are described by Siemens in [27], [26] and [28]. The Siemens methods follow two ISO standard testing methods. ISO standards 10140 describe the measurement of the transmission loss in two reverberation chambers with a microphone setup for both rooms. A second measurement method, which is used when the RR is an anechoic chamber, is using a sound intensity probe to measure the sound intensity level behind the test object. A standardised measurement is described in ISO 15186. The methods of the intensity measurement are described in ISO 9614. There can either be done an intensity scan over the test surface or a measurement on mesh points. [28]

6.1.1 Measurement equipment and setup of the measurement room

Listed here is the equipment used for the measurement:

- Microphone calibration: Larson Davis Cal200
- Microphone capsule: PCB 377B02

- Microphone pre-amplifier: PCB 426E01 ICP TEDS 378B02
- Microphone stands
- BNC connection cables
- SMB-BNC connection cables
- Yamaha XDR10 loudspeaker
- XLR speaker cable
- XLR-TRS cable
- LMS SCADAS Mobile SCM05
- Software Simcenter Testlab 2021.2
- Sound Intensity Probe: BSWA MPA221, Spacer 12 mm
- Sound Intensity calibrator G.R.A.S. Type 51AB

In figure 6.1 the connection of the equipment devices is displayed. On the input channels 1 to 4 the four microphones are connected. Channel 1 and 2 go into the source room, channel 3 and 4 are connected with the microphones in the receiving chamber. Channel 5 and 6 are connected with the intensity probe. Channel 5 is the microphone, which is placed close to the test object and in the direction of the sound propagation. The BNC cables need to be switched to SMB connectors. The same applies to the XLR connection. That was switched to TRS adapter and to BNC to then fit the SMB connection.

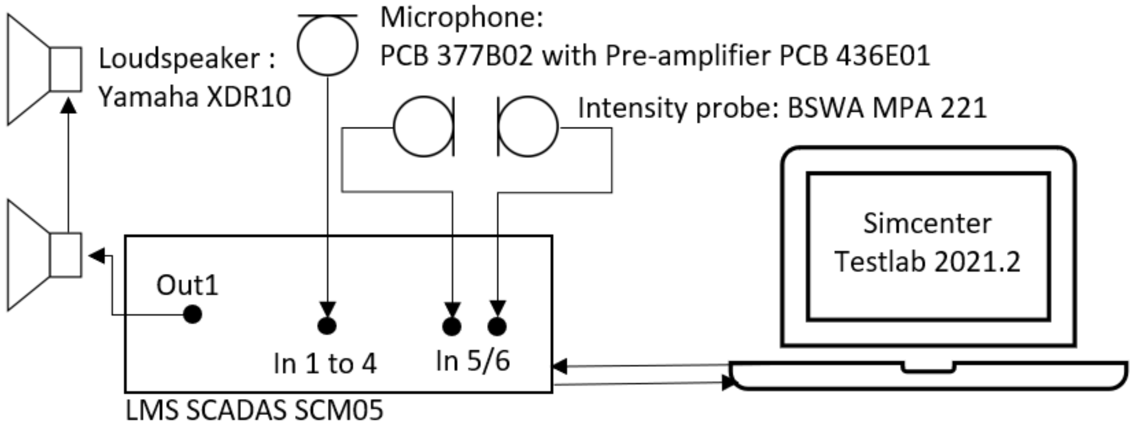

Figure 6.1: Connection of the measurement equipment

The arrangement of the loudspeaker and microphones in the rooms was following the guidelines set by the ISO 10140 standards. The minimum distances for the space between the microphone and loudspeakers and the rooms boundaries are proposed. For the microphone positions it is suggested to have at least 0.7 m distance between the microphones and to the room boundaries or reflective surfaces. For the distance to the source and the test object 1 m distance is defined. [8]
For the source position 0.7 m space between the loudspeakers and the room boundaries is suggested. Furthermore, the two loudspeakers need to have a difference of 0.1 m in their height. [9]

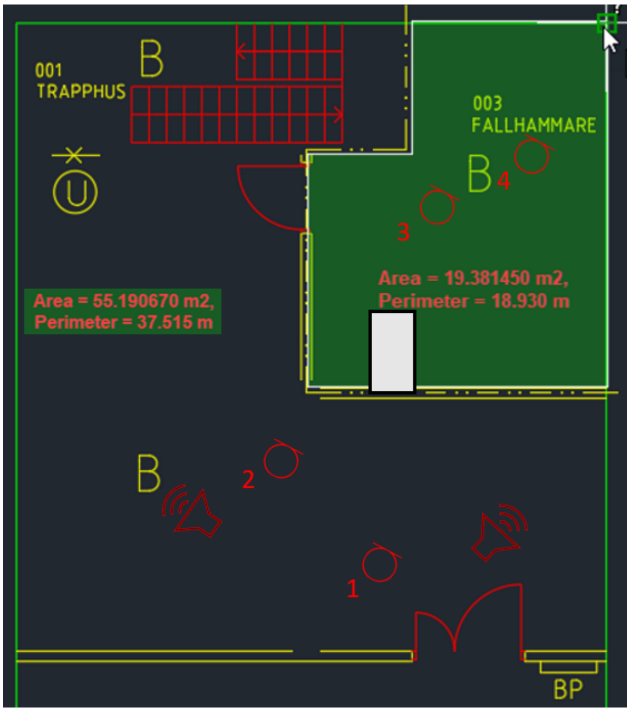

Figure 6.2: Sketch of the measurement rooms and the source and microphone positions

Instead of using four microphones per room, only two microphone positions were measured. As a consequence, the average measured in the room has lower accuracy and the sound pressure variations in the room are not fully measured and included in the average.
The distribution of the equipment in the rooms is sketched in figure 6.2. In figures 6.3 and 6.4 the setup in the source and receiving chamber is presented. For the arrangement of the loudspeakers in the source room, it was important to assure, that the sources radiated in different directions to assure diffuse field conditions.
The source room, which is a reverberation chamber, has a room volume of $193.17\,\mathrm{m}^3$.
The receiving chamber has a room volume of $67.83\,\mathrm{m}^3$ and is semi-anechoic.
The duct was extended into the RR. This reduced the chances of breakin noise.

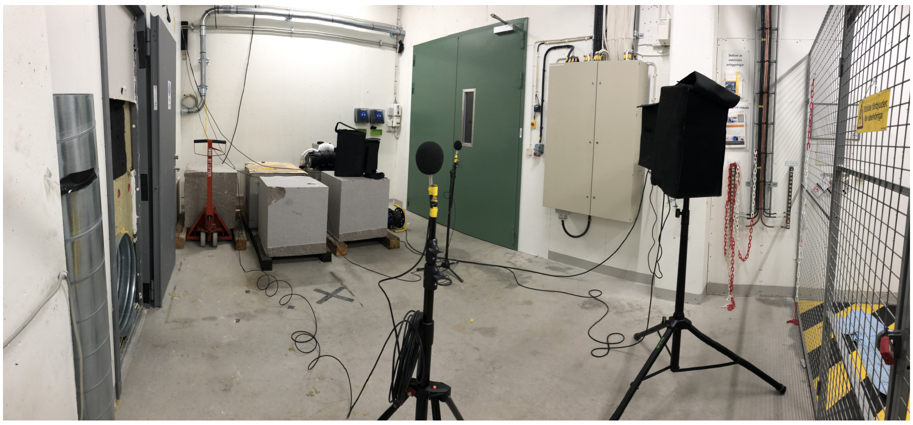

Figure 6.3: The measurement rooms and the source and microphone positions

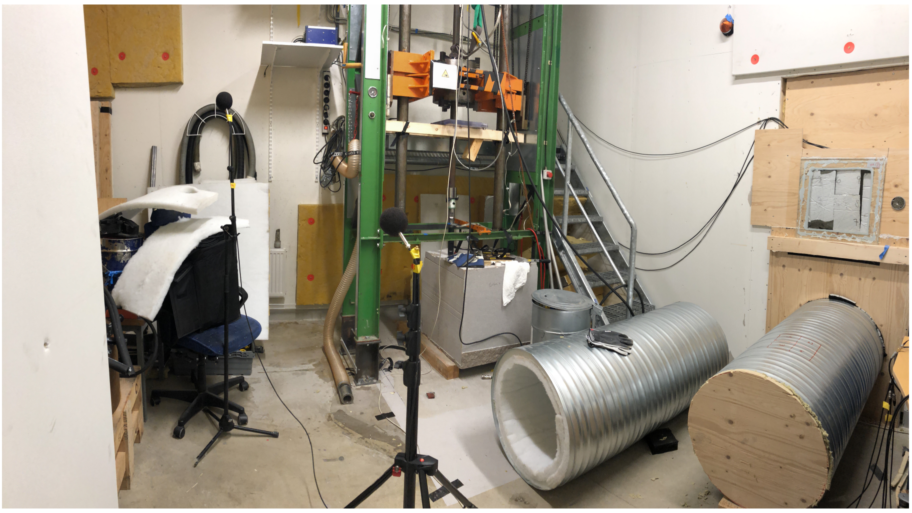

Figure 6.4: The measurement rooms and the source and microphone positions

6.1.2 Measurement Procedure

After setting up the microphones and the loudspeakers as it is described in section 6.1.1, the software Simcenter Testlab 2021.2 can be setup for conducting the measurements. For the pressure measurement the Testlab application "Sound Transmission Loss Testing using rooms" was used.
The signal processing settings were set to a bandwidth of 10 240 Hz and 8192 spectral lines, which results in a frequency resolution of 1.25 Hz. And the measurements were averaged over a duration of 10 s.
For the intensity method, the application "Intensity Testing" was set up. A 12 mm spacer was used, which gives valuable results in a frequency range from 125 Hz to 6.3 kHz. [29] The signal processing settings were set to a bandwidth of 6400 Hz and 5120 spectral lines, so that the frequency resolution is 1.25 Hz.
For the point method the duct outlet was divided into four equal sections and the measurement points were on the centre of those sections for 10 s each. The intensity scan over the cross-section of the scale model was done over 90 s.
The source signal was set to pink noise.
During the setup of the software the calibration for the microphones and the sound intensity probe was conducted.
Furthermore the atmospheric conditions of the room were measured.

The measurement cases, which were measured are listed below. Different cases were measured to investigate the test environment and the setup of the duct in the partition. Another part of the investigations was to see if the pressure measurement gave similar results as the intensity measurement. Also the intensity measurement methods - scanning and point method - were compared.

- Background Noise
- closed test window in SR and closed and sealed duct in RR
- open test window in SR and closed and unsealed duct in RR

- open test window in SR and closed and sealed duct in RR
- open test window in SR and open and unsealed duct in RR
- open test window in SR and open and sealed duct in RR
- duct wall, open test window in SR and closed and sealed duct in RR
- duct with absorber
- duct with absorber and perforated plate

The sound pressure level or respectively the sound intensity levels L measured on the microphone positions in the rooms or on the mesh points n were A-weighted and averaged following equation 6.1.

$$L_{avg} = 10\log_{10}\frac{1}{n}\Sigma 10^{\frac{L_i}{10}} \tag{6.1}$$

The TL using the room-method is determined with equation 6.2 from the level difference of the averaged sound pressure level in the source room L_{SR} and the averaged sound pressure level in the receiving room L_{RR}. The correction factor consists of the area of the duct cross-section S and the equivalent absorption area A. [7]

$$TL = L_{SR} - L_{RR} + 10\log_{10}\frac{S}{A} \tag{6.2}$$

The equivalent absorption area A is calculated by the RR volume V and the reverberation time T of the RR . [8]

$$A = 0.16\frac{V}{T} \tag{6.3}$$

For the TL determination using the intensity probe the averaged sound pressure level in the SR L_{SR} and the sound intensity level L_I behind the test object in the RR are used.
Equation 6.4 shows how to calculate the TL using an intensity probe. [5] When adding the absorption layer and the perforated plate, the area of the cross section in the source room S_{SR} differs from the scanned cross section in the receiving room S_{RR}, so a correction is added to the equation:

$$TL = L_{SR} - L_I + 10\log_{10}\frac{S_{SR}}{S_{RR}} - 6 \tag{6.4}$$

For the measurement of the sound transmission of the duct wall, the surface area of the duct in the RR was inserted to S_{RR}.

6.2 Measurement Results

In the following the results to the conducted measurements are discussed.

The atmospheric conditions in the measurement room are displayed in the table 6.1 below.

Table 6.1: Atmospheric condition in the RR during the measurements

Temperature	18.8 °C
Humidity	33.4 %
Air pressure	1012 hPa

The results of the reverberation time measurement were provided and are listed in table 6.2 below.

Table 6.2: Reverberation time T_{60} in the receiving chamber

125 Hz	0.47 s
160 Hz	0.60 s
200 Hz	0.28 s
250 Hz	0.31 s
315 Hz	0.29 s
400 Hz	0.26 s
500 Hz	0.25 s
630 Hz	0.24 s
800 Hz	0.24 s
1000 Hz	0.27 s
1250 Hz	0.26 s
1600 Hz	0.28 s
2000 Hz	0.28 s
2500 Hz	0.29 s
3150 Hz	0.26 s
4000 Hz	0.32 s
5000 Hz	0.27 s
6300 Hz	0.29 s
8000 Hz	0.26 s

The background noise was sufficiently low, so that no correction had to be conducted.

The pressure measurements were conducted for a frequency range from 31.5 Hz to 8 kHz, but the behaviour of the scale model could best be evaluated from 125 Hz to 6.3 kHz because in this range the TL results were broader over the frequency range. Above and below, the sound pressure just decreased strongly.

6.2.1 Investigation of the measurement environment

The results about the study of the test setup are displayed in figure 6.7. The transmission through leakages between the test window and the test object and the contribution of the outlet (duct opening side in the receiving room) of the duct in the RR were measured. Furthermore the TL of the duct wall was measured with the intensity probe. For that a 20 cm × 20 cm area was marked and divided into four parts, see figure 6.5.

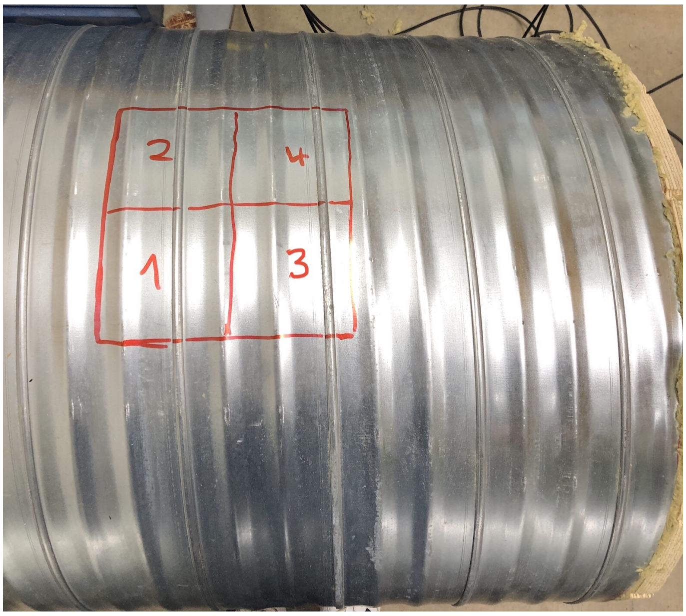

Figure 6.5: Points for sound intensity measurement to determine the transmission from the duct wall

This small area was selected instead of scanning the whole duct. In the measurement room was not enough space around the duct to place the intensity probe and conduct the scanning. Also, it was assumed, that the duct's outer walls radiate equally, so that it is possible to make a projection by increasing the area factor S_{RR} of equation 6.4.
The duct's outlet opening and the leakages around the test window were closed, so that for this measurement case, the sound transmission into the RR is mostly coming from the duct wall. The central point of each of the four parts was measured with the intensity probe. The result displayed in figure 6.7 is the average over all four points. Below 1 kHz the energy was not measurable and therefore did not give useful results.

Usually the partition window is sealed by a double-wall construction of wooden boards and absorptive material. For the duct measurement an opening was cut in. During the measurement the duct was placed into the partition window and the gaps between the duct wall and the partition window were sealed with absorptive material. Furthermore, the outlet of the duct was sealed with the cutout from the partition wall, which consisted of a thick layer of absorptive material and a wooden board. In the source room the inlet opening of the scale model was sealed by shutting the metal door of the test window. For better understanding the setup is photographed in figure 6.6. The duct was not lined with the absorber at this point. For the investigation of the measurement environment the setup was reduced bit by bit.

Figure 6.6: Setup to the study of the measurement environment: the gaps between the duct and the test window were sealed and the outlet was closed. In the source room the door to the test window was closed.

The upper black curve in figure 6.7 displays the case, which gives the highest possible TL for this test setup. In the source room the window is closed by the metal door and in the receiving room the duct outlet opening is closed and the leakages are sealed from both sides of the test window. Overall the curve follows the mass law (see figure 4.9) until 1 kHz. Above 1 kHz, the curve dives to a minimum at 1.6 kHz. The TL increases over the whole frequency range from 10 dB up to 35 dB. There is a maximum at 160 Hz. The maximum at low frequencies goes back to the room's reverberation time and the correction factor of the TL. The minimum at 1.6 kHz is most likely due to leakages, for example, the door list. Both will be investigated further below.

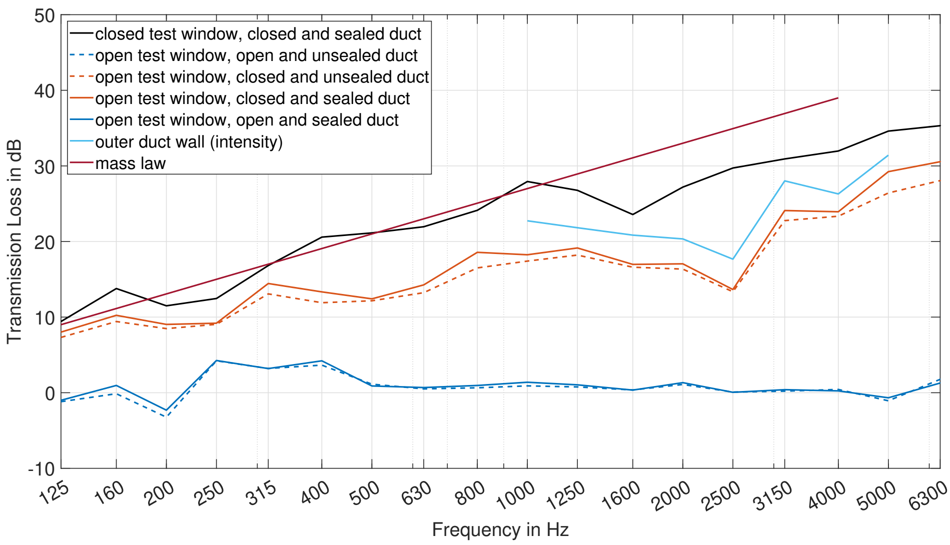

Figure 6.7: Results to the study of the measurement setup regarding leakages and the distribution of the sound from the outlet opening of the duct

From the black (closed inlet and outlet) to the red solid curve the inlet of the duct or the door in the source room to the partition window is opened again. So, opening the inlet side of the duct lowers the TL between 125 Hz and 315 Hz around 3 dB. Above 315 Hz the difference between the curves increases up to a value of 16 dB at a 2.5 kHz minimum. At even higher frequencies, the difference decreases again.

Since the outlet is still closed, the transmission into the receiving room goes over the duct wall. This can be seen from the similarity to the intensity measurement conducted on the outer duct wall. This means the red curve shows breakout noise radiated from the duct into the RR by exciting the duct wall just like the light blue curve. The breakout noise measured from the intensity probe is about 3 dB higher. The offset between the intensity and the pressure measurement can be due to the position of the microphones in the RR or the dependency of the intensity result on the area.
From the raw data of the measurement an offset between the pressure measured at microphone position 3 and 4 can be observed. Microphone 3 might still be placed to close to the duct outlet, so that it is still in the acoustic near field. On the other hand, the intensity measurement is very dependent on the area S_{SR} and S_{RR}. To fit this measurement to the pressure measurement, the area factor was not calculated with the 0.2 m × 0.2 m area, but with the entire outer duct wall area. This assumes, that the whole outer duct wall can be represented by the smaller measured section. It is however possible, that there are still some surfaces contributing to the sound radiation. The duct is placed very close to the hard, reflecting floor, which could increase the radiation from the duct. A possibility here, is that radiated sound gets reflected at the floor and influences the pressure measured at the probe. To investigate this theory further more area was added to S_{RR}. With adding 3 m^2 the curves from the intensity and the pressure measurement can be fitted. The result is shown in figure 6.8 through the dark red curve.

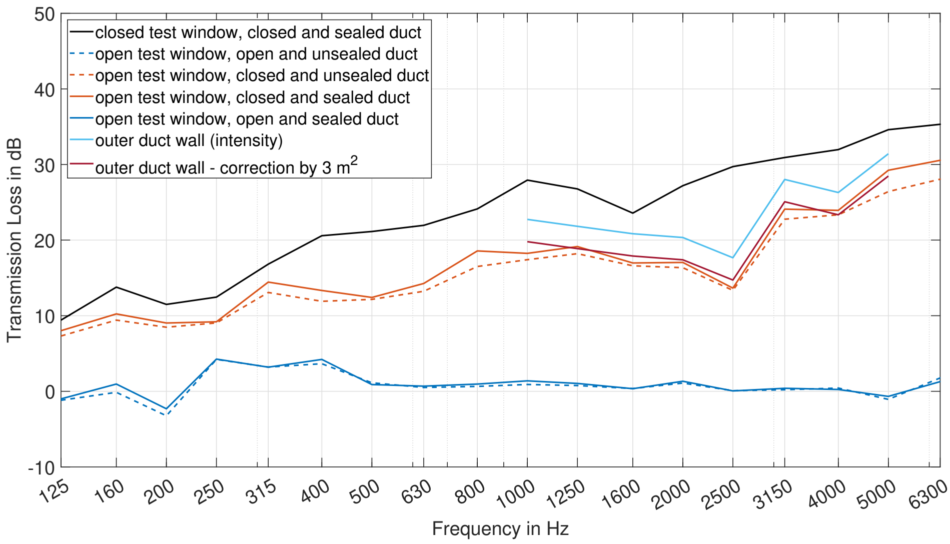

Figure 6.8: Results to the study of the measurement setup regarding leakages and the distribution of the sound from the outlet opening of the duct with correction

The three curves (figure 6.7) representing the break out noise have a characteristic frequency minimum at 2.5 kHz in common.

At last, the duct opening in the receiving room is opened as well. The results are displayed in blue. In the lower frequencies there are some minima and maxima in the duct. Above 500 Hz the curve is rather broad an shows a very low TL.

Between the dotted and the solid curves, the influence of sealing is represented. Sealing the duct into the partition window improves the TL by approximately 2 dB. So, an influence from leakages can be seen, but it does not contribute all that much to the transmission.

As mentioned, there are different frequency minima and maxima, that can be observed in the measurement of the test environment.
Different mechanism play a role in the generation of those frequency maxima.

Especially in the low frequency range up to 500 Hz most of the minima and maxima go back to local disturbances in the measurement rooms. The rooms, where the measurements were conducted, are not specially designed test facilities, where good care was taken to get the sound field sufficiently diffuse at low frequencies. With the duct in the partition between the rooms coupling can occur, which leads to global modes. Furthermore does the absorption in the RR at low frequencies influence the TL results.

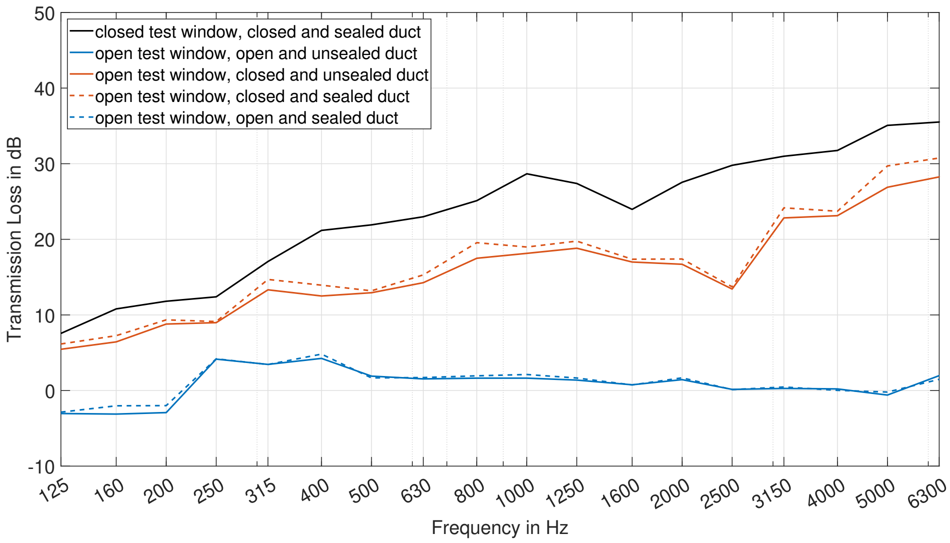

Figure 6.9: Results to the study of the measurement setup regarding leakages and the distribution of the sound from the outlet opening of the duct with adjustment to the average reverberation time

For example, do the curves of figure 6.7 all show a maximum at 160 Hz and a minimum at 200 Hz. But when looking back at the pressure measured in the receiving and source room for this frequency it can be seen, that both pressure curves are broad and do not show any characteristic frequency. This means, that the frequency minimum is a consequence of the correction factor for the absorption in the RR. When re-calculating the TL with the average reverberation time, which is 0.3041 s, the frequency curve is broader. The maximum at 160 Hz vanishes, so its value is more similar to 200 Hz. This can be observed in the low frequency range of figure 6.9. The reverberation time differs most from the average at 125 Hz and 160 Hz (compare to table 6.2). The RR is less absorptive for this frequency range.

The most prominent minimum for the measurement presenting the closed-inlet/closed-outlet case (black) is at 1.6 kHz. Here the course of the curve dips away from the mass law (see figure 6.7). The measurement room does not fulfil ISO standard requirement. It is most likely that leakages occur in the test setup, from which sound components get transmitted into the RR. A weak spot of the test room is the door list of the metal door, which can be closed in the SR in front of the partition window.

The measurements representing the breakout noise have a strong frequency component at 2.5 kHz. Like the minimum at 1.6 kHz this frequency is also not a strong component of the signal measured in the SR. Hence, it is induced by the transmission path. In the case for the outer duct wall, this frequency minimum shows the ring frequency f_r of the duct. The ring frequency f_r can be calculated by the speed of longitudinal sound waves c_L (steel: c_L= 5050 m/s) in the structure and the duct diameter d [22]:

$$f_r = \frac{c_L}{\pi d} \tag{6.5}$$

For this duct, the calculated ring frequency is 2550 Hz.

When looking at the TL of the open duct, it can be observed, that in the low frequency range, the reduction is higher between 250 Hz and 400 Hz. Above the reduction is rather low as expected. The minima below 200 Hz go back to the low absorption in the RR. Between 250 Hz and 400 Hz possibly modes of the coupled system can be observed.

The most important finding from these measurements is, that there are a lot of room influences, which make it hard to adequately describe the low frequencies.

6.2.2 Investigation of the measurement method

There are two different measurement procedures that are described for the TL determination when using rooms. The ISO 10140 standard is commonly used for two reverberation chambers. And the intensity probe is used for an anechoic receiving chamber and a reverberant source room. Because both methods can be used in this setup, they were compared to see if one is more advantageous. Furthermore, the measurement setup can be validated by comparing the results.

From the previous investigations, it was already know, that there are room influences and coupling between the test rooms, which influence the results up to 500 Hz. The measurements were performed in a semi-anechoic receiving chamber. So, its not the usual kind of acoustic test room used to conduct TL measurement according to ISO 10140. For the pressure method a diffuse sound field with at least four microphones would be desirable to get a good average of the room. It has to be assessed if there are disadvantages in the pressure method when using the semi-anechoic chamber.

The intensity probe measures the acoustic energy radiated from the duct opening, so it could be expected, that the RR has only little influence on the test result. Furthermore, the intensity scanning and point method were conducted to find out about possible differences in the results.

The spacer determined the frequency range of the intensity probe. The results are valid for a frequency range from 125 Hz to 6.3 kHz. Due to some restrictions in the LMS software, the pressure on the microphones could only be recorded up to the 5 kHz octave band instead of 6.3 kHz.

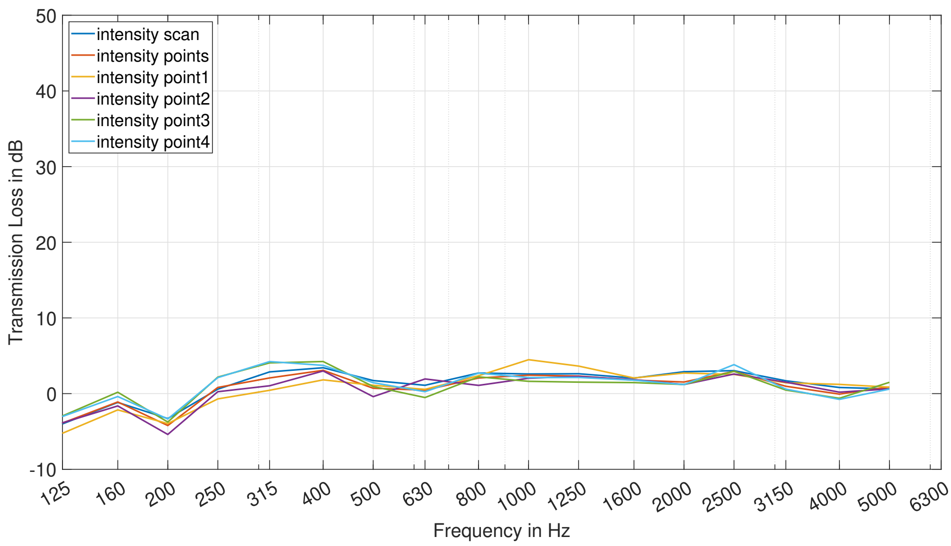

Figure 6.10: Comparison between the intensity scanning method and the point method for the measurement of the open duct sealed in the partition window

In figure 6.10 the result of the comparison between the intensity scan over the cross section and measurement of mesh points and averaging is compared. One can see, that the measured points vary a bit. But the averaged result and the intensity scan match quite good. This can be observed better in figure 6.11. The agreement could probably be increased further if more points were measured and averaged.

In figure 6.11 the TL of the open duct, which is sealed into the partition window, is displayed. This time the results obtained from the two intensity methods and two pressure results are compared. A small difference in the magnitude can be observed in the low frequency range between 125 Hz and 315 Hz. The maxima in the pressure results are slightly higher in their magnitude by around 4 dB. Overall there is a good agreement between the curves and the methods for this case.

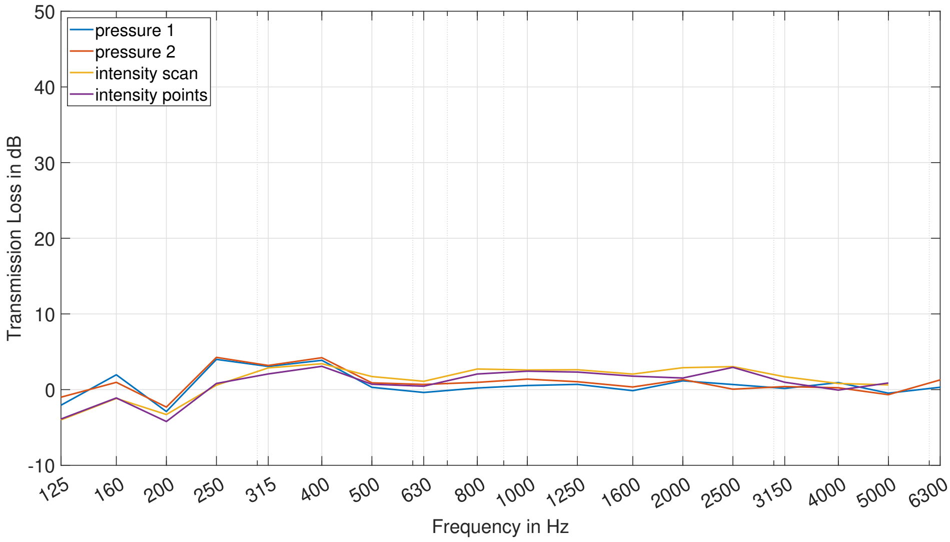

Figure 6.11: Comparison of the results obtained for the open sealed in duct with the pressure measurement and the two intensity methods

In figure 6.12 the results from the pressure measurement are also compared to the intensity point method, but for the case of the absorber in the duct and the absorber with the perforated plate. Compared to the results shown in figure 6.11 for the open duct, the measurements now show more deviations between the pressure and intensity TL.

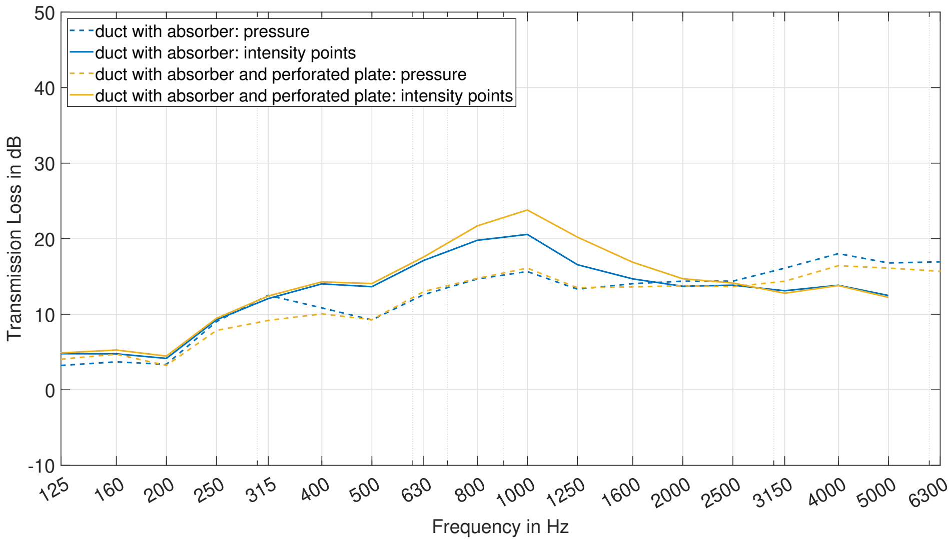

Figure 6.12: Comparison of the results obtained from the pressure and intensity method for the duct with absorber and the duct with absorber and perforated plate

Until 315 Hz the agreement between the curves is quite good. In the frequency range from 315 Hz to 2.5 kHz the intensity method delivers much higher TL values than the pressure measurement. Above 2.5 kHz that behaviour switches. The TL of the intensity values decreases, which is odd because it does not follow the usual mass law, while the TL pressure values are now higher than the TL intensity values.

Another observation that can be made from this graphs is the behaviour of the perforated plate and that both measurement methods give different indications. From the pressure method, it can be concluded, that there is almost no advantage in the use of the perforated plate with the absorber. There are frequency ranges, where the absorber alone performs better.

The intensity method gives an entirely different observation. Here the perforated plate with the absorber gives a higher TL for the frequencies between 630 Hz and 2 kHz. Otherwise -above and below that frequency region- there is no difference between the absorber alone and with the perforated plate.

This matching or mismatching of the curves was investigated under exclusion of the pressure measured at microphone 3. The results are displayed in figures 6.13 and 6.14. For the measurement of the open duct (figure 6.13), the duct with the absorber and the duct with the absorber and perforated plate (figure 6.14), the difference between the intensity and pressure results was investigated in connection to the placement of the microphones in the RR. During the measurements microphone 3 was placed closer to the duct and might be positioned in the near field of the duct. To compare to the pressure measured in the far field, only the results from microphone 4 are included in figures 6.13 and 6.14 for the pressure method.

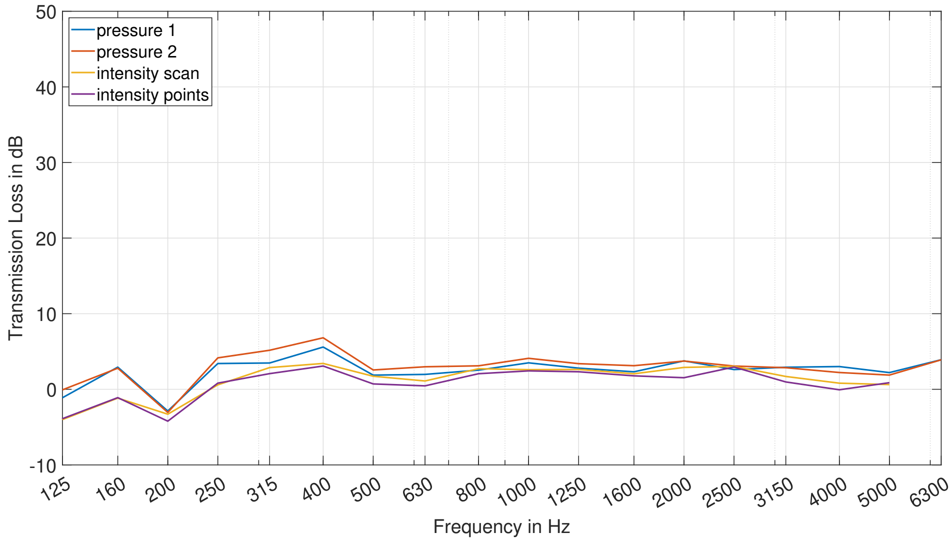

Figure 6.13: Comparison of the results obtained for the open sealed in duct with the pressure measurement and the two intensity methods, the microphone on position 3 was excluded from the pressure results

For the measurement of the open duct in figure 6.13 a better agreement between

125 Hz and 315 Hz is achieved. In the frequency range above, the curves of the different methods match quite well.

When looking at figure 6.14 for the lined duct cases, the difference between the TL from the pressure measurement and from the intensity measurement decreases around 1 kHz. It can also be observed, that the course of the curve is similar except for the high frequency range, where the TL of the intensity decreases in comparison to the TL of the pressure measurement. Possibly more measurement positions in the RR could lead to a better average and maybe a more similar result.

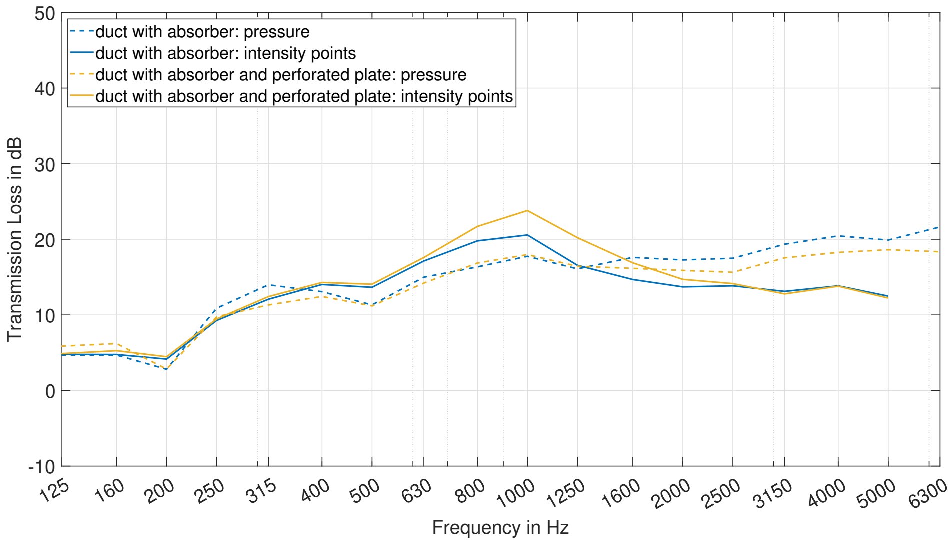

Figure 6.14: Comparison of the results obtained from the pressure and intensity method for the duct with absorber and the duct with absorber and perforated plate, the microphone on position 3 was excluded from the pressure results

To sum up, one can say, that there is no difference in the TL results between using the intensity scan or point method. However, using the pressure or intensity method has shown to deliver different results with increasing complexity of the silencer. For the open, empty duct the measurement results had a good agreement. But when the absorber and the perforated plate were added, the differences increased. In the low frequencies both methods have the same trend, but towards high frequencies the differences increase.

An advantage of the intensity method is, that it is not so dependent on the placement of the measurement position in the room as long as the probe is held in the right position around the test object. This was seen, when only the microphone furthest in the receiving room was compared to the intensity result instead of averaging the result from the pressure method with the second microphone. It was found out, that during the measurements the microphone on position 3 was too close to the scale model. The agreement between the intensity result and the pressure measured on position 4 was much better.

More measurement positions in the room would have helped to get a better average of the room. Furthermore, the positioning of the microphones should have been adjusted. To get better measurements conditions for the pressure method, it is also possible to cover the absorptive material and add reflective walls. With this the diffuse sound field could have been improved, so that the placement of the microphones is not as sensitive.

A further aspect, that might have lead to the difference between the intensity and the pressure method, is the area, which is scanned for the intensity measurement. It is possible, that not only the duct opening in the RR contributes to the sound field measured by microphone 3 and 4. The breakout noise was already discussed before and contributes to the sound field. If the scanned area S_{RR} is increased by the duct wall area, the match could be improved.

Another difference between the methods was seen by the effect of the perforated plate. The intensity method result showed an advantage of having the perforated plate, while the pressure measurement did not show an effect by inserting the plate to the silencer. From the measurement of the AVH90, when the circular perforations were compared to the squared holes (figure 2.11), it was concluded, that there is some reducing effect by having circular perforations. Although one needs to be aware, that this was measured and concluded for flow conditions. Even though the effect of going from no perforated plate to inserting a perforated plate was not measured on the full-sized machine, the results of the squared holes to circular holes investigation indicates, that there should be an advantage to having the perforated plate. It is possible, that the effect increases, when flow is added to the silencer, so the pressure method might also pick it up. A separate investigation, for example, in an impedance tube can give an idea on what to expect regarding the effect of inserting a perforated plate like the one used in the scale model.

6.2.3 Behaviour of the Scale Model

For the measurement of the scale model, the ventilation duct used for the scale model was measured step by step. From the simple duct to the duct walls lined with absorption material and finally with the absorber and the perforated plate. The results are displayed in figure 6.15.

It can be observed, that the TL of the empty duct is low. The curve was already discussed regarding the resonant behaviour in the low frequency range.

Then the absorber is lined on the duct wall. This increases the over all TL. Here the curve shows some strong minima or maxima in the low frequency range up to 500 Hz, which go back to the previously described room influences. At 1 kHz and 4 kHz the TL shows some maxima in the curve, where the absorption is stronger.

For the absorber and the perforated plate, the curve looks the same. The effect from the perforated plate in the pressure measurement is rather small. There is no advantage in using the perforated plate from this results. It is possible, that the properties change, when flow is induced to the silencer.

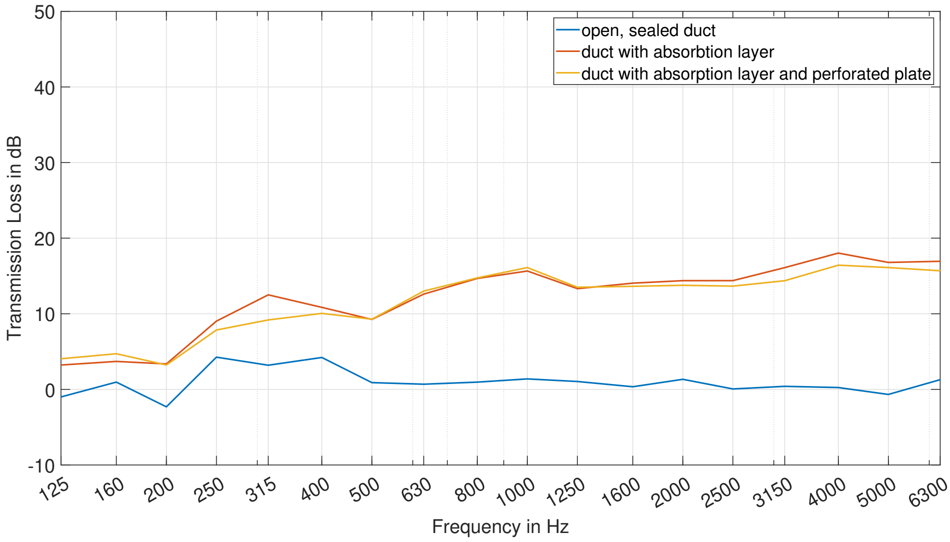

Figure 6.15: The comparison of the TL results from the pressure method of the scaled silencer model from duct to the added absorber and the duct with the absorber and the perforated plate

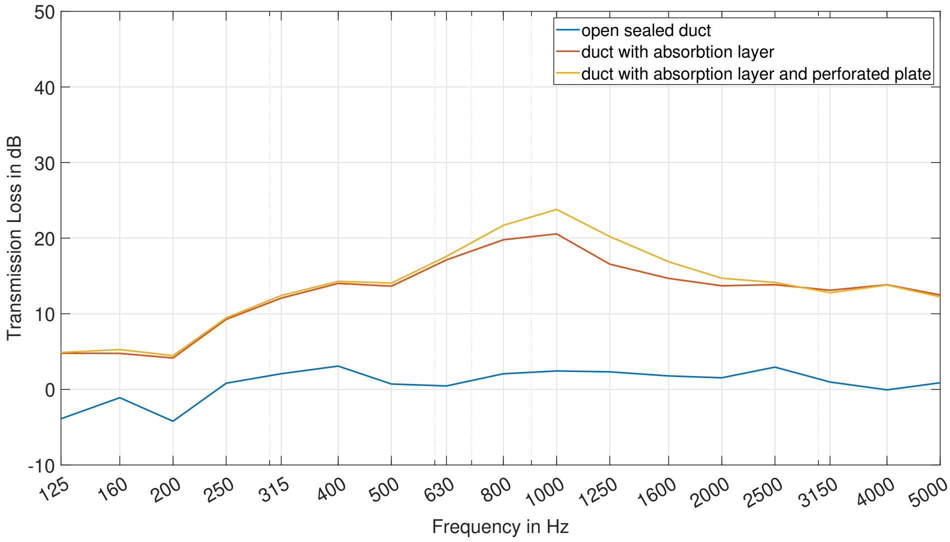

Figure 6.16: The comparison of the TL results from the intensity method of the scaled silencer model from duct to the added absorber and the duct with the absorber and the perforated plate

The results on the TL from the intensity method is in the low frequency range similar to the pressure method results. Then they differ quite a lot in regards of a higher TL for the intensity method and showing differently strong influences by the perforated plate. This was already previously discussed. Some of the differences were due to the placement of the microphones in the room. The difference shown by the perforated plate needs to be investigated further. From the measurement of the AVH90 an effect by the circular perforations was shown under flow conditions. But its unclear what to expect for this case and a separate study was suggested.

The prominent noise reduction at 1 kHz might go back to different wavelength fitting the duct diameter and the duct length. A quarter of the length of the duct corresponds to a frequency of 1046 Hz. And half a wave fits the diameter of the duct. That corresponds to 1079 Hz. This is an assumption, that could be investigated further by measuring the pressure distribution over the length of the duct or over the diameter.

The theory on round silencers predicted the highest noise attenuation when the frequency fitted the passage of the duct for waves propagating from an axial direction into the silencer duct. With the absorber and the perforated plate the passage is 0.488 m in diameter. When following the theory of [22], the maximum attenuation should be achieved for 696 Hz for a normal incident field. The measurement result represents the behaviour under diffuse field conditions. The maximum attenuation was observed around 1 kHz. A possibility, that would need further investigation is, that the frequency of maximum attenuation shifts under diffuse field conditions and when the sound enters the silencer from all directions.

6.3 Measurement of Insertion Loss

In the second measurement a more direct radiation into the duct was tested. This was achieved by placing a loudspeaker source closer to the duct's inlet opening. The distance between the source and the duct was 1 m. The setup is shown in figure 6.17.

The measurement equipment is the same as before. Only the microphones 1 and 2 and the second loudspeaker in the SR are no longer needed. The software setup is the same. This measurement was conducted in the 'Sound Intensity Testing' software of Testlab.

In this second measurement setup the silencer was again measured bit by bit: from the empty duct to the duct lined with the absorber and then with the absorber and the perforated plate.

As the incident sound field is now less defined, the IL was determined by the sound level measured in the RR or from an intensity scan on the outlet opening of the duct. The IL was calculated between the empty duct and the duct with the absorber or the duct with the absorber and the perforated plate. Additionally the TL was determined again, but this time by the intensity scan on the inlet and outlet opening. From the intensity the sound power values were determined with the area of the cross-section. The power results were than inserted to equation 4.21.

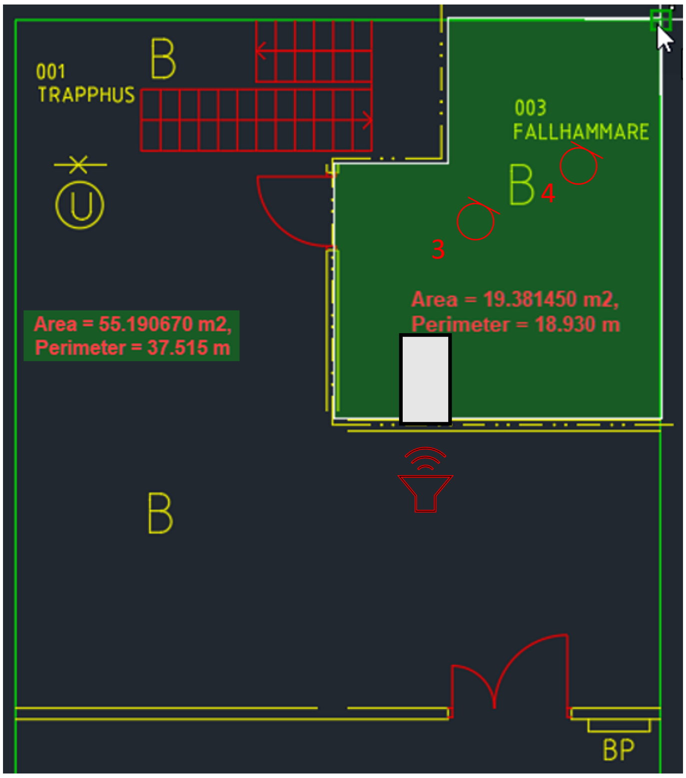

Figure 6.17: Sketch of the measurement rooms and the source and microphone positions for the second measurement

In figure 6.18 the results of the calculation of TL are displayed. Similar to the results in 6.15, there is a very low change between the sound power levels between the inlet opening and the outlet opening for the empty duct. Around 1 kHz the TL is negative, which leads to the conclusion, that the sound at the outlet is higher than at the inlet. This could be due to a $\lambda/4$ mode fitting the duct length of 1.3 m. The frequency of a quarter of 1.3 m is 1046 Hz. Another possibility is that half the wavelength of the duct diameter fits the diameter of the duct. This frequency is 1079 Hz.

Adding the absorber and the absorber with the perforated plate, increases the TL. So that there is noise reduction from the inlet to the outlet side. The level difference increases strongly around 1 kHz. This was also found in the TL measurements before. The perforated plate adds a little noise reduction below 1 kHz.

The IL results could be derived from pressure and intensity results, so both of them are presented in figure 6.19. The curves of the intensity method are similar in shape like the corresponding curves in figure 6.18. But the silencer with the absorber and the perforated plate (yellow curve) shows lesser performance than the silencer with the absorber only (blue curve). This is similar to the results of the TL measurement in figure 6.15. There the absorption layer alone was better than the absorber together with the plate. Here is a very small advantage at low frequencies up to 630 Hz. In the results from the pressure measurement, the effect of the perforated plate is rather small.

However the results between the intensity and pressure methods differ. They have a good agreement until 630 Hz, then they begin to deviate and above 1.6 kHz the difference becomes bigger.

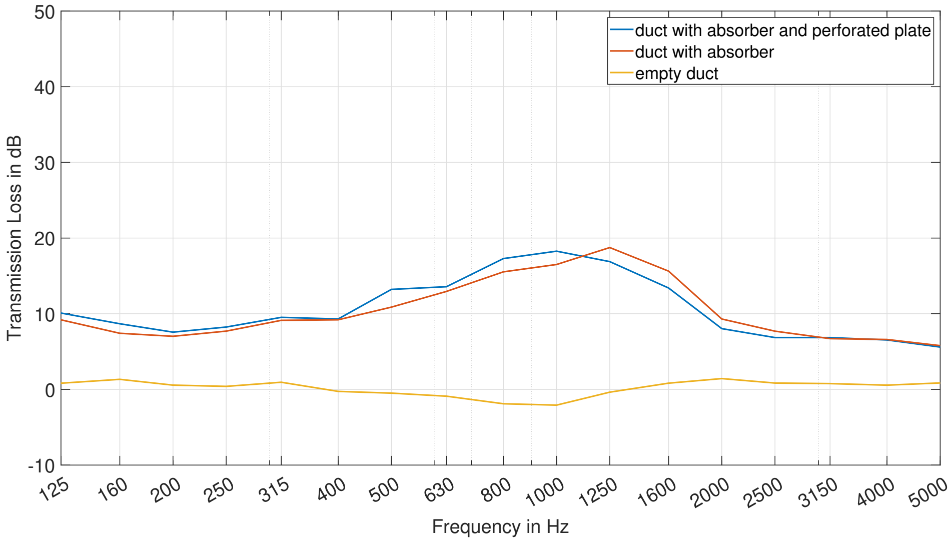

Figure 6.18: TL from the intensity scan at the inlet and outlet side of the duct

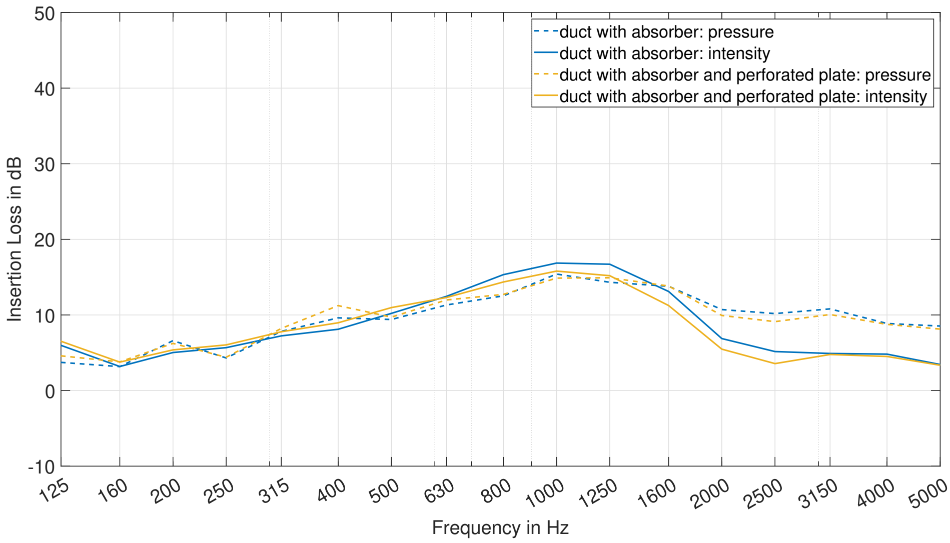

Figure 6.19: IL obtained from pressure and intensity measurements of the duct with absorber and the duct with absorber and perforated plate compared to the empty duct

It is possible to make a rough comparison of the IL of the scale model and the AVH90. Here the IL from the measurement, where the perforated plate was covered by the solid reflective plate, can be used to make a first comparison (see figure 2.5). For the AVH90 the IL is rather low for frequencies below 125 Hz. Above

125 Hz the IL increases to a maximum at 400 Hz with approximately 18 dB. Towards higher frequencies the IL decreases. The shape of the curve is the same for the AVH90 and the scaled silencer. The IL of the scaled silencer also increases until a maximum value. Instead of 400 Hz the maximum value for the scale model is reached at 1000 Hz. Again one has to be aware, that the results from the AVH90 are representing the behaviour under flow conditions.

6.3.1 Conclusion on the Measurements

In the following the most important findings from the measurements are briefly summarized.

The measurements, which were performed to investigate the measurement setup and the environment, showed that the measurement rooms are not ideal at low frequencies up to 500 Hz. Also, the results are very dependent on the microphone position. The measurement representing the breakout noise showed a high transmission loss, so its influence on the further measurements is low. Possibly the breakout noise from the duct will get even more reduced, when the absorber is added.

Furthermore, the results showed that the influence from leakages around the test object is rather low. But still there are minor contributions, so the sealing of the leakages was conducted for all further measurements.

The comparison of the different measurement methods, showed that the TL results from pressure and intensity differ. This goes back to the measurement positions of the microphone in the RR. An other possibility, that could help to decrease the difference, is scanning the entire duct in the RR. With increasing S_{RR}, the TL values should decrease. Then they might match better with the pressure curve.
An advantage in the use of an intensity probe is, that it is not so dependent on the room properties. The probe can be moved close to the test object to get the local TL. Room influences, leakages or other influences from the test environment do not have such a strong influence. For the intensity method there is no preferred method. Both, the point and the scanning method, delivered results of good agreement.

Also, the IL is a good way to describe the reduction achieved by the silencer. It is not so much dependent on the incident field.

The duct measurements show no transmission loss by the empty duct as expected. When the absorber is added, the TL and IL show an increase especially around 1 kHz. This higher transmission loss is measured in both measurement setups and with both measurement methods.
When the perforated plate is added to the absorber, there are differences in the result of the pressure and intensity measurement. While the pressure measurement gives almost no further reduction, the change by the perforated plate is more profound when doing intensity measurements.
From the investigations on the perforations of the AVH90 it was expected, that the

perforated plate shows absorbing properties for a resonance frequency. Its possible, that this can be seen better under flow conditions. To be able to better estimate, what to expect from this perforated plate, the absorber and the plate could be investigated in an impedance tube. Then one can go back to the test results and see, which match better with the impedance tube results.

7
Acoustic Simulation

A simulation of the scaled silencer was created to be able to test new noise mitigation measures beforehand in the future. In the following chapter it will be described how the Finite Element Method (FEM) was used to conduct the simulation. And a comparison to the measurement results will be done.

7.1 Setup of the Simulation Model

The simulations were conducted with the software Comsol Multiphysics 6.1.
In the following the setup of the model will be described. The model was built in 3D space dimensions and the physics interface used was "Pressure Acoustic, Frequency Domain". The information on the Comsol study and nodes can be found in [3].

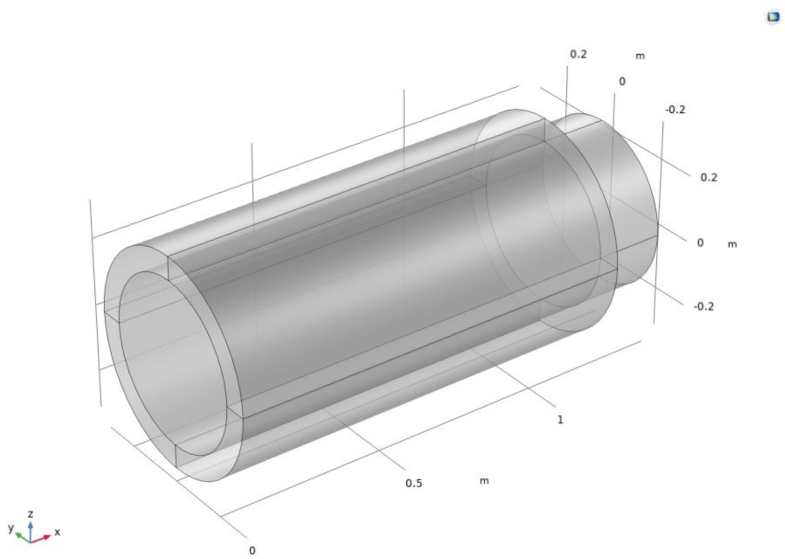

Figure 7.1: The model of the acoustic simulation

The first step is to set up the object, that was analysed. For the geometry a solid cylinder of 0.63 m diameter and 1.4 m length was set up. Under axis "x-axis" was chosen to place the cylinder horizontally. Then a layer of 7 cm was added to the sides. The layer will represent the cavity, which is filled with the absorptive material.
A work plan was added parallel to the inlet of the duct with an offset of 1.2 m, so it would fit the silencer length. Then the duct was parted there, so that a domain

with 0.2 m length is behind the model of the scaled silencer. The domains created by the layer can be deleted. This 0.2 m long area will be a "Perfectly Matched Layer", so that the waves leaving the duct will be absorbed. The geometry is displayed in figure 7.1.

Under "Materials" air is added to the geometry domains.

Then the "Pressure Acoustics, Frequency Domain" physics study was set up. The "Plane Wave Radiation" node was added and applied to the inlet boundary of the silencer. Under "Incident Pressure Field" the amplitude of the incident plane wave is set to 1. The simulation was performed for a normal incident.

For the outlet side a "Boundary Probe" was added under "Definitions". It will give out the average absolute pressure on the boundary.

To describe the layer, which was added in the geometry, a "Poroacoustics" node was added. The "Poroacoustics" node was set up to use the empirical equations model of Delany and Bazley, to solve for the losses of the porous material. The only model input needed is the flow resistivity of the material. The flow resistivity had to be estimated for the simulation because there was no data on that available from the supplier.

The flow resistivity was determined by simulating an impedance tube and conducting a parameter sweep over different resistivity values. The porous material layer in that impedance tube simulation also was 7 cm long and was solved by the Delany and Bazley model as well. A plane wave was inciding into the duct by using the "Port" function. Then the absorption coefficient was calculated from the reflection factor, which was determined by the power of the incident and reflected wave. The absorption coefficient result for the different resistivity values could then be compared roughly to a measured absorption coefficient of the material under diffuse field conditions. Unfortunately no data for a normal incident was available. The resulting absorption coefficients are displayed in section 7.2.
The flow resistivity added to the model of the scaled silencer was $6000\,\mathrm{Pa}\cdot\mathrm{s/m^2}$.

At last the "Interior Perforated Plate" node was added. This model solves for the impedance of the holes. The "thin plate" model was chosen. This neglects the losses due to heat conduction. The holes of the plate have a triangular pattern, so the porosity is calculated by the following equation:

$$\sigma = \frac{\pi d_h^2}{2\sqrt{3}a^2} \tag{7.1}$$

with d_h being the hole diameter, a the center-to-center distance between the holes [22]. In this study d_h is 5 mm, a is 2 * 2.5 mm radius + 3 mm spacing. So, the porosity is σ is 0.354.
When the physics model was set up, the mesh was built. A "free triangular" mesh was applied to the circular areas. Then that was swept over the geometries length.

The mesh size was set to "extra fine", which gave a maximum element size of 0.049 m.

In the frequency domain study the simulation was solved from 100 Hz to 2000 Hz in steps of 10 Hz.
The TL is evaluated from the simulation. It can be calculated by the pressure amplitude from the incident wave field, which was 1, and the boundary probe, which solved the absolute pressure: $10 \cdot log10(1/bnd)$.

7.2 Simulation Results

In figure 7.2 the results that were obtained during the estimation of the flow resistivity are displayed. It is difficult to compare the results measured in diffuse field to the simulation results for normal incident. The absorption coefficient in the low frequency region is much lower for the plane wave excitation. Furthermore, the used Delany and Bazley model is known to give lower estimations for the absorption coefficient compared to the absorption coefficient that one would obtain from a measurement. To be able to choose one of the values, a short research was conducted to find out if other suppliers had published flow resistivity results of comparable materials. From the values found for other polyester fibers 12 000 $\mathrm{Pa} \cdot \mathrm{s/m^2}$ seemed unreasonably high. With regard to the density of the material 6000 $\mathrm{Pa} \cdot \mathrm{s/m^2}$ seemed to be a good choice. But a confirmation can only be made by a measurement of the material in an impedance tube.

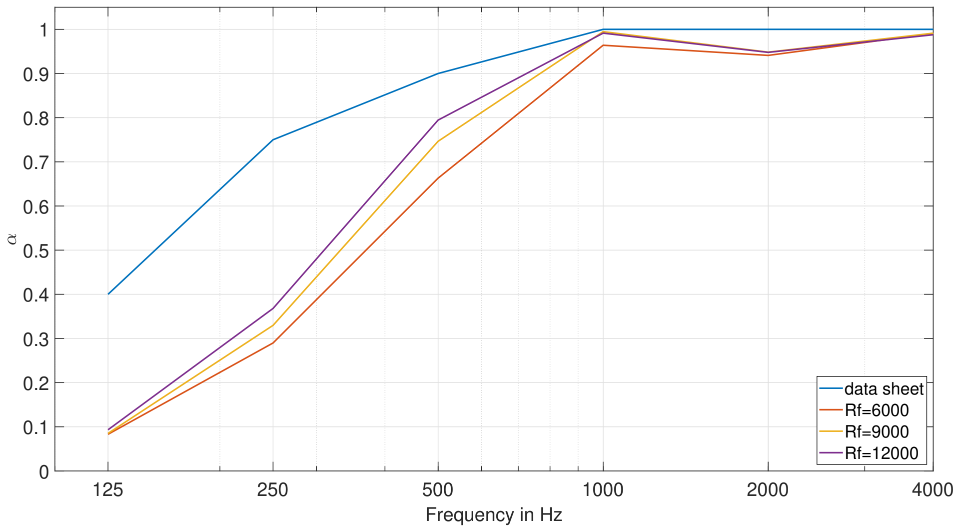

Figure 7.2: Determination of the flow resistivity by comparison of measurement data and simulation results

The results of the simulation are displayed in figure 7.3. The simulation was conducted for a simple cylindrical duct, the duct with only the "Poroacoustics" node and with the "Poroacoustics" and the "Interior Perforated Plate" nodes. As it was described in chapter 4.2, there is no decrease in amplitude for plane waves propagating in a duct. Hence, there is no TL for the empty duct. With adding the

"Poroacoustics" node, the TL increases to a peak around 700 Hz and then decreases again. According to the theory on round silencers in chapter 4.3.4, the maximum attenuation should be achieved, when the diameter of the passage fits the wavelength. The diameter of the passage in the model is 0.49 m or 0.488 m with the perforated plate. Hence, the maximum attenuation should been achieved around 693 Hz or 696 Hz. So, there is an agreement between the theoretical model of [22] and the simulation model.

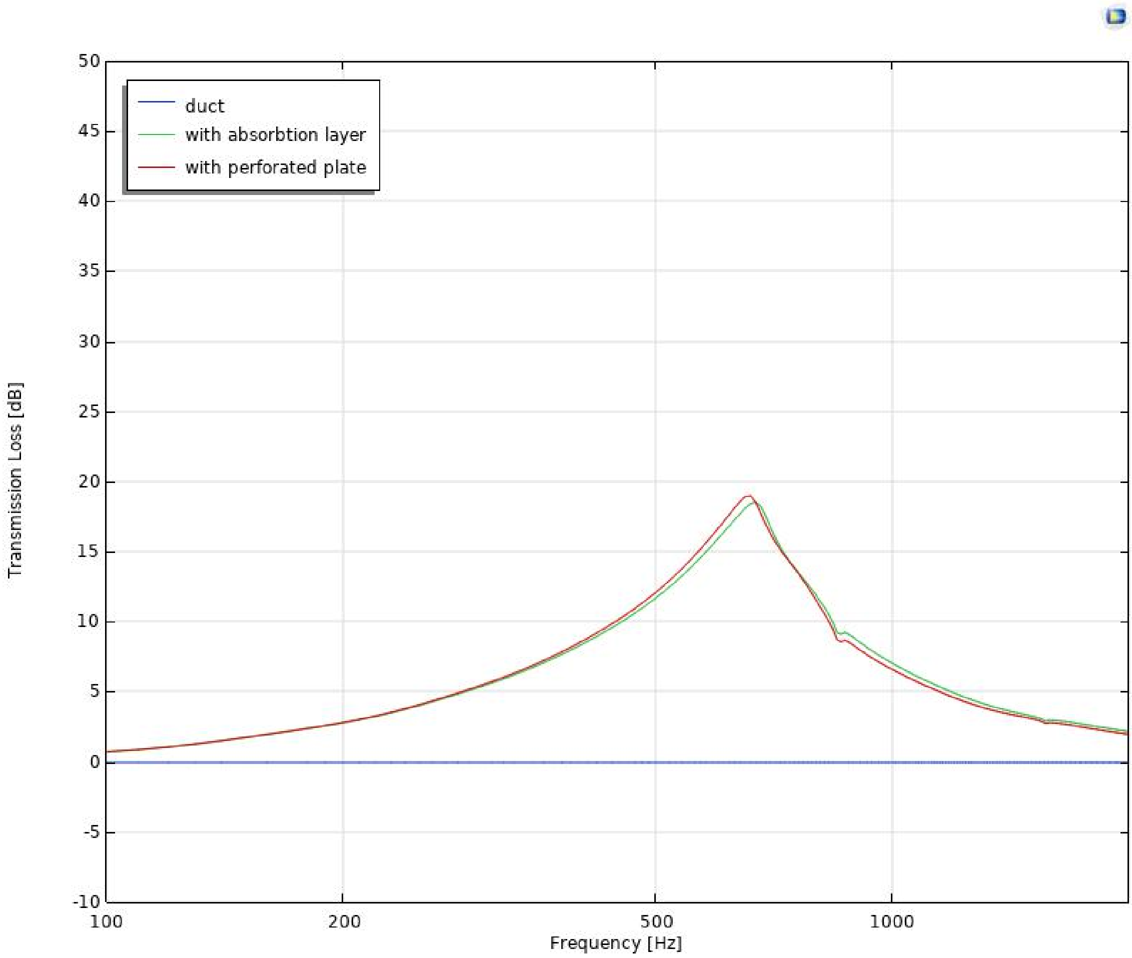

Figure 7.3: TL result from the acoustic simulation model for the empty duct, the duct lined with absorber and the duct lined with absorber and the perforated plate.

Another observation that can be made from the displayed result is the effect of the perforated plate. In the simulation the perforated plates adds very little to the sound reduction. The curve representing the result of the duct with the absorber and the perforated plate seems a bit shifted towards lower frequencies compared to the curve showing the TL of the duct with only the absorber. This leads to a small effect by the perforated plate below the resonance peak. And above the resonance peak the TL of the duct with the absorber exceeds the TL values of the duct with the perforated plate added on the absorber.

This behaviour could also -but a bit stronger- be observed in the results of the second measurement setup, where the TL was determined by the intensity scan of the inlet and the outlet opening of the silencer duct (see figure 6.18).

The result from the simulation was summed up into octave bands and compared to the TL results from the 2 measurement setups. In figure 7.4 the results obtained from the pressure measured at the microphone positions in the first setup are compared to the simulation results. In figure 7.5 the comparison to the TL determined by the intensity measurement is shown. And at last figure 7.6 compares the TL from the simulation to the TL measured with the intensity probe in the second setup.

When comparing the similarity between the three different TL results and the simulation result, it can be observed that the results from the pressure method reach lower TL values (see figure 7.4), while the TL obtained from the intensity method in the first measurement are higher compared to the simulation (see figure 7.5). A good agreement can be observed for the intensity scanning in the second measurement setup. The measurement of the inlet and outlet seems to better represent the boundaries calculated in the simulation (see figure 7.6). Here also the magnitude of the TL values are similar.

Both, the measurements and the simulation, have a strong attenuation for one frequency component in common. The measurement results all showed a strong attenuation in the 1 kHz frequency band, while the simulation has the strongest attenuation in the frequency band of 630 Hz. The result of the simulation agrees with the calculation presented in [22]. Possibly, the frequency of maximum attenuation shifts under diffuse field incident. This could be studied further by extending the current simulation model with multiple incident angles.

Overall the simulation shows a good trend of the curve and is therefore sufficiently comparable. Below 500 Hz, the measurement results indicate problems with the measurement room, so of course they do not appear in the simulation.

There are a few aspects, that contribute to the difference between the measurement results and the simulation.

As mentioned before the use of the Delany and Bazely model comes with some uncertainties. Their model is strongly dependent on the flow resistivity, which was difficult to choose for the model as the absorption coefficient between the simulated impedance tube and the data sheet with the diffuse field sound absorption coefficient vary. With that the chosen flow resistivity of $6000\,\mathrm{Pa}\cdot\mathrm{s/m^2}$ might not fully represent the model. Here it also comes into account, that the material is compressed by the perforated plate, which influences the density of the fiber material. This can be improved by conducting measurements in an impedance tube for the used fiber material.

The differences are also due to the different incident fields in the simulation and in the measurements. The measurements picture multiple incident directions, while the simulation shows the expected results for normal incidence. So, the flow resistivity might show different attenuating properties dependent on the incident angle. In the impedance tube the wave incides on the surface of the fiber material. In the scale model the sound propagating into the silencer model incides on the side of the absorption material instead. On the sides, the pressed layers separate more easily, so the flow resistivity might be different there. Furthermore, the material is a little bit compressed by the perforated plate, which leads to a change in the density.

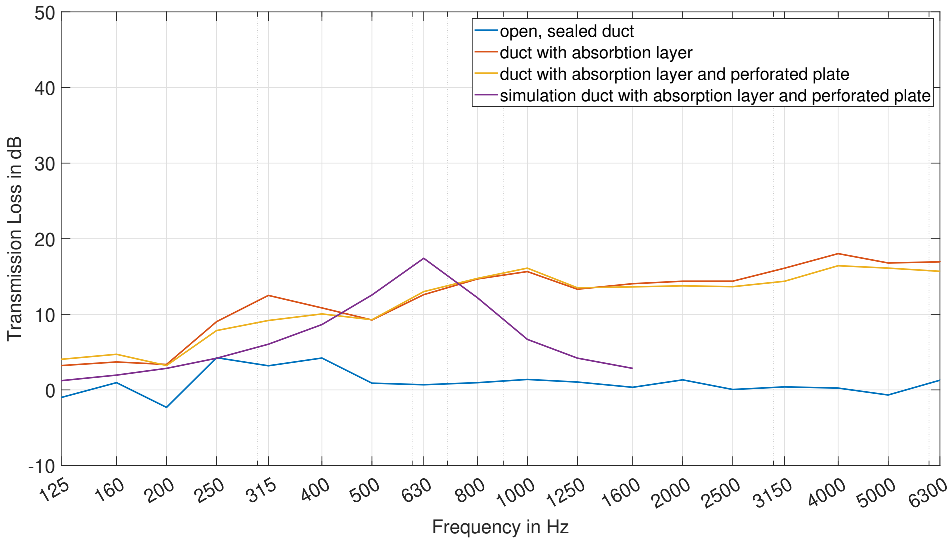

Figure 7.4: The TL result of the simulation compared to the TL result from the pressure measured in the first measurement setup

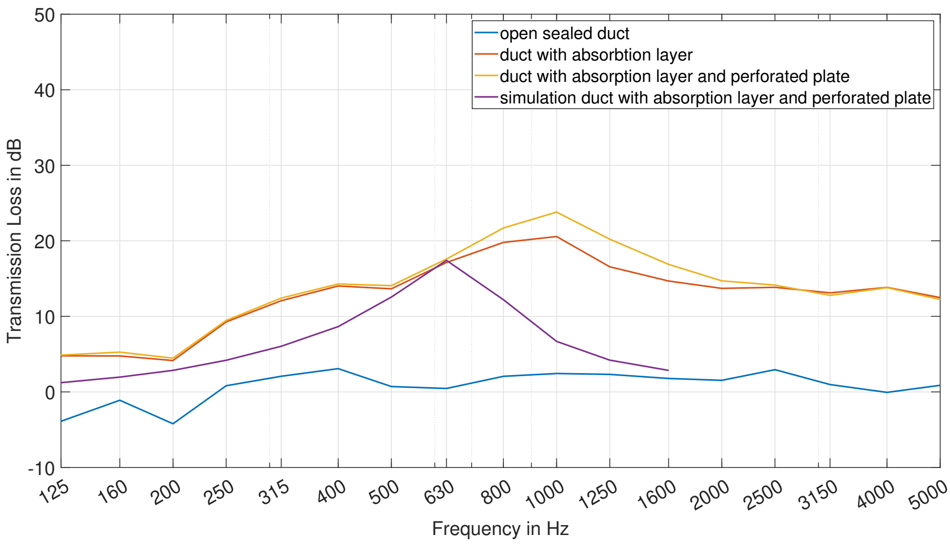

Figure 7.5: The TL result of the simulation compared to the TL result from the intensity measured in the first measurement setup

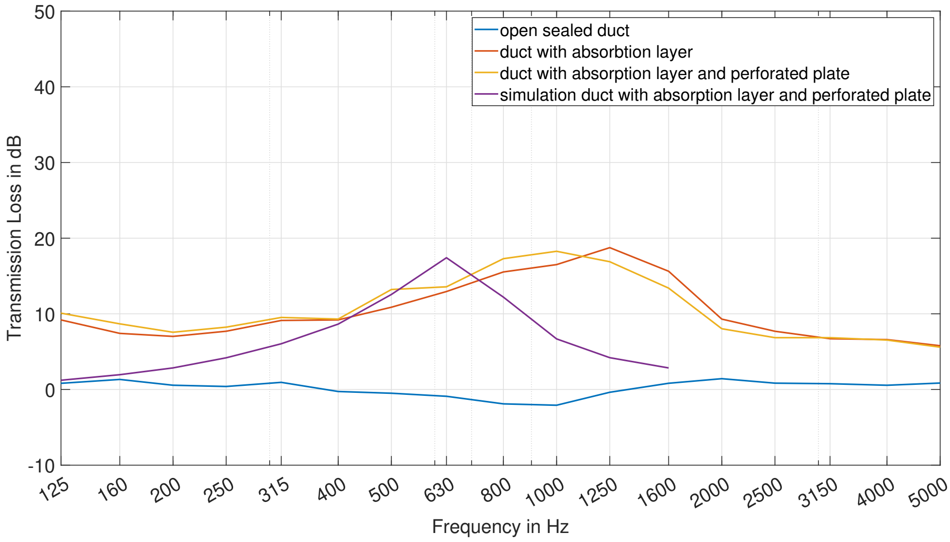

Figure 7.6: The TL result of the simulation compared to the TL result from the intensity measured in the second measurement setup

8 Conclusion

8.1 Summary of the Findings

From the investigations on the fan and flow parameters it could be concluded, that the kinematic similarity in regard to Mach and Reynolds number is sufficient when scaling the AVH90 ventilation system. On the other hand the acoustic similarity is low due to the expected shift in BPF because of the weaker motor in the scale model. A change in the number of blades in the scale model can help to reproduce the same BPF.

The investigations on the measurement environment showed a high influence of the room, especially for low frequencies. Therefore the intensity measurement is probably easiest to used as it is not so strongly dependent on the surroundings. There was no observable difference between the intensity point method or the intensity scanning method.

When adding the absorber and perforated plate to the empty duct the overall TL could be increased. The strongest attenuation of the incoming noise was achieved around 1 kHz. The difference between having only the absorber in the duct or the absorber together with the perforated plate gave different indications. The pressure method did not show any strong effects, which differed from the intensity results. More investigations need to be done to see what can be expected by adding the perforated plate, to draw better conclusions.

When creating the FEM simulation, the flow resistivity of the material had to be estimated, which showed to be difficult. The available data was obtained under different incident field conditions than how it was possible in the separate impedance tube simulation for the parameter sweep.
Anyway, the agreement between the simulation and the measurements was good as it could represent the general trend of the TL. The adding of the perforated plate lead to a little shift of the TL in the simulation. It leads to slightly higher TL values for the silencer with the perforated plate at low frequencies, but an advantage by the absorber alone at frequencies above the peak. In the second measurement setup, where the speaker was placed closer to the duct and the TL was determined by the intensity scanning of the inlet and outlet opening, the same behaviour could be observed.

However, the frequency of maximum attenuation was different. For the measurements it was in the 1 kHz frequency band instead of the 630 Hz frequency band. The difference might be due to the different incident fields or the used model for the absorption layer, which has some uncertainties.

8.2 Future Work

In the continuation of the project after the thesis the fan and guide vanes should be attached to the scale model to complete it. Then the behaviour of the silencer can be investigated under flow conditions.

Suggestions regarding the design on the scaled fan and the expected flow and fan parameter were already given. But for the practical implementation decisions regarding the BPF or the number of blades should be made. Also, the meaning of scaling the fan by 1.85 instead of 1.84 to keep the tip clearance needs to be understood further. Maybe a CFD simulation of the entire scale model can be executed to see the difference in the aerodynamic properties and draw better conclusion regarding the aerodynamic similarity between the models.

Then the studies presented in the thesis regarding the acoustic sound transmission can be redone under flow conditions. It can be expected, that the acoustic properties presented here, will change under flow conditions. Maybe the perforated plate, which did not show a big effect, will have an impact on the sound reduction like it was measured for the AVH90.
There also is the possibility to attach the centrum-baffle. But one needs to be aware, that even though the liner dimension were not scaled, the baffle would probably need to be scaled to fit the geometry of the scaled inner duct. The scaling of the baffle would help to get the space between the duct and the baffle scaled by the scaling factor to fulfil similar aerodynamic geometry. The kinematic and dynamic similarity should be investigated for this case as well.

When the scale model is completed, the emitted sound could be measured and compared to the measurements done on the AVH90 to see if the noise treatment in the scale model can sufficiently represent the reduction it has on the real machine and if it is a good way of assessing whether a noise treatment has a noise reducing effect and therefore gives a good indication on the performance it might have in the full-sized system. When the comparison between the AVH90 and the scale model is satisfying, the comparison can be extended to Epiroc´s further ventilation products. Then it can also be studied if the current noise treatment needed to be fitted to the duct- and fan size.

For the use of the acoustic simulation in the future to investigate changes on the silencer it should be extended to also be able to evaluate higher modes and multiple incident direction. Another way -which would be even closer to the measurement setup- would be to define a random pressure field with multiple incident angles for the incident boundary. This would be more similar to the diffuse field in the measurement setup. If the acoustic model delivers good results it can be extended further, to compute the TL under flow conditions.

Furthermore, other noise mitigation measures could be tested. If one aims for the reduction of the emitted noise from the ventilation system, a good achievement can probably be made, by reducing the BPF and the harmonics.
Here the Tyler-Sofrin-rule could for example be investigated further. There are 11 guiding vanes at the moment. To fulfil the Tyler-Sofrin rule 16 or more guide vanes are needed. Another measure to directly reduce the fan noise could be to investigate the irregular spacing of the fan blades.
Then secondary measures could be tested. There is an opportunity to reduce the inflow disturbances for example by placing the motor on the downstream side. This would reduce the turbulence on the inlet side and result in noise reduction due to less flow separation.
Also new silencer designs can be investigated. Different studies were presented in chapter 3. The use of a MPP in the silencer could be investigated like in the paper [16]. This could also be tested in combination with petal-shaped perforations instead of round perforations [32]. Also interesting is the use of AM like in [20] or [34].
With the investigations on different noise treatments, it can also be studied further, if the noise treatment needs to be fitted to the fan size.

Bibliography

[1] The Reynolds Number. https://www.jousefmurad.com/fluid-mechanics/the-reynolds-number/.

[2] Understanding fan acoustics | Processing Magazine. https://www.processingmagazine.com/home/article/15587087/understanding-fan-acoustics.

[3] Acoustics Module User's Guide. Technical report, 1998. www.comsol.com/blogs.

[4] CFD Module User's Guide. Technical report, 1998. www.comsol.com/blogs.

[5] Byggakustik – Mätning av ljudisolering ibyggnader och hos byggnadselement medljudintensitet –Del 1: Laboratoriemätning(ISO 15186-1:2000) Acoustics – Measurement of sound insulationin buildings and of building elements using-sound intensity –Part 1: Laboratory measurements(ISO 15186-1:2000). Technical report, 2003. www.sis.se.

[6] Akustik-Bestämning av ljudeffektnivåer och ljudenerginivåer för bullerkällor med användning av ljudtryck-Teknisk metod för frifältsförhållanden över en reflekterande yta (ISO 3744:2010) Acoustics-Determination of sound power levels and sound energy levels of noise sources using sound pressure-Engineering methods for an essentially free field over a reflecting plane (ISO 3744:2010). 2010. www.sis.se.

[7] Byggakustik-Mätning av ljudisolering hos byggnadselement i laboratorium-Del 2: Mätning av luftljudsisolering (ISO 10140-2:2021) Acoustics-Laboratory measurement of sound insulation of building elements-Part 2: Measurement of airborne sound insulation (ISO 10140-2:2021). 2023. www.sis.se.

[8] Byggakustik-Mätning av ljudisolering hos byggnadselement i laboratorium-Del 4: Mätprocedurer och krav (ISO 10140-4:2021) Acoustics-Laboratory measurement of sound insulation of building elements-Part 4: Measurement procedures and requirements (ISO 10140-4:2021). Technical report, 2023. www.sis.se.

[9] Byggakustik-Mätning av ljudisolering hos byggnadselement i laboratorium-Del 5: Krav på provrum och utrustning (ISO 10140-5:2021) Acoustics-Laboratory measurement of sound insulation of building elements-Part 5: Requirements for test facilities and equipment (ISO 10140-5:2021), 2023. www.sis.se.

[10] A. P. Dowling and J. E. Ffowcs Williams. *Sound and Sources of Sound*. 1983.

[11] Sabry Allam and Mats Abom. Noise Reduction for Automotive Radiator Cooling Fans Effect of Speed Breaks on Vehicle Dynamics and Ride Comfort View project. Technical report, 2015. https://www.researchgate.net/publication/272175821.

[12] Ockert P.H. Augustyn, Sybrand J. Van Der Spuy, and Theodor W. Von Backström. Numerical and experimental investigation into the accuracy of the fan scaling laws applied to large diameter axial flow fans. *Proceedings of the Institution of Mechanical Engineers, Part A: Journal of Power and Energy*, 230(5):477–486, 8 2016.

[13] Bernard Massey and John Ward-Smith. *Mechanics of Fluids*. Stanley Thornes (Publishers) Ltd., 7 edition, 1998.

[14] Loz Blain. Toroidal propellers: A noise-killing game changer in air and water. https://newatlas.com/aircraft/toroidal-quiet-propellers/.

[15] Charlie Bricault, Yang Meng, and Sébastien Goudé. Optimization of a silencer design using an helmholtz resonators array in grazing incident waves for broadband noise reduction. *Applied Acoustics*, 201:109090, 12 2022.

[16] Felix Czwielong, Sebastian Floss, Manfred Kaltenbacher, and Stefan Becker. Influence of a micro-perforated duct absorber on sound emission and performance of axial fans. *Applied Acoustics*, 174, 3 2021.

[17] Con Doolan and Danielle Moreau. *Flow Noise*. Springer Nature Singapore, 2022.

[18] Epiroc Rock Drills AB. Underground ventilation | Serpent ventilation fans | Epiroc. https://www.epiroc.com/en-me/products/ventilation-systems/serpent-fan-system.

[19] Walter Frei. Which Turbulence Model Should I Choose for My CFD Application? | COMSOL Blog, 2017. https://www.comsol.com/blogs/which-turbulence-model-should-choose-cfd-application/.

[20] Jingwen Guo, Renhao Qu, Yi Fang, Wei Yi, and Xin Zhang. A phase-gradient acoustic metasurface for broadband duct noise attenuation in the presence of flow. *International Journal of Mechanical Sciences*, 237, 1 2023.

[21] H P Wallin, U Carlsson, M Abom, H Bodén, and R Glav. *Sound and Vibration*. Stockholm.

[22] István L. Vér and Leo L. Beranek. *Noise and Vibration Control Engineering - Principles and Application*. John Wiley & Sohns, Inc., 2 edition, 2006.

[23] Jack E Made and Donald W Kurtz. N A Review of Aerodynamic Noise From Propellers, Rotors, and Lift Fans. 1970.

[24] Mats Abom. *An introduction to Flow Acoustics*. Stockholm, 4 edition, 2012.

[25] Christof Ocker, Thomas F. Geyer, Felix Czwielong, Florian Krömer, Wolfram Pannert, Markus Merkel, and Stefan Becker. Permeable leading edges for airfoil and fan noise reduction in disturbed inflow. *AIAA Journal*, 59(12):4969–4986, 12 2021.

[26] Siemens. Measuring Sound Transmission Loss Using Rooms, 8 2019. https://community.sw.siemens.com/s/article/Measuring-Sound-Transmission-Loss-Using-Rooms.

[27] Siemens. Sound Transmission Loss, 10 2019. https://community.sw.siemens.com/s/article/sound-transmission-loss.

[28] Siemens. Simcenter Testlab: Measuring Sound Intensity, 2 2020. https://community.sw.siemens.com/s/article/Simcenter-Testlab-Measuring-Sound-Intensity.

[29] Siemens. Sound Intensity, 2020. https://community.sw.siemens.com/s/article/Sound-Intensity.

[30] A.A Taratorin and A.B. Mukhametov. Acoustic and Aerodynamic Properties of the Petal-shaped Absorption Silencers. pages 1–5. Institute of Electrical and Electronics Engineers (IEEE), 11 2022.

[31] W T W Bill Cory. *Fans & Ventilation - A Practical Guide*. Roles & Associates Ltd and Elsevier, 2005.

[32] Zhimin Xu, Wei He, Xiangjun Peng, Fengxian Xin, and Tian Jian Lu. Sound absorption theory for micro-perforated panel with petal-shaped perforations. *The Journal of the Acoustical Society of America*, 148(1):18–24, 7 2020.

[33] Hua Dong Yao, Zhongjie Huang, Lars Davidson, Jiqiang Niu, and Zheng Wei Chen. Blade-Tip Vortex Noise Mitigation Traded-Off against Aerodynamic Design for Propellers of Future Electric Aircraft. *Aerospace*, 9(12), 12 2022.

[34] Tingsheng Zhong, Cheng Yang, and Mats Åbom. Tonal noise reduction of an electric ducted fan using over-the-rotor acoustic treatment. *Applied Acoustics*, 205, 3 2023.

DEPARTMENT OF ARCHITECTURE AND CIVIL ENGINEERING
CHALMERS UNIVERSITY OF TECHNOLOGY
Gothenburg, Sweden
www.chalmers.se

CHALMERS
UNIVERSITY OF TECHNOLOGY